Continuous change detection and classification of land cover using all available Landsat data

Zhe Zhu *, Curtis E. Woodcock

Center for Remote Sensing, Department of Earth and Environment, Boston University, 675 Commonwealth Avenue, Boston, MA 02215, USA

ARTICLE INFO

ABSTRACT

A new algorithm for Continuous Change Detection and Classification (CCDC) of land cover using all available Landsat data is developed. It is capable of detecting many kinds of land cover change continuously as new images are collected and providing land cover maps for any given time. A two-step cloud, cloud shadow, and snow masking algorithm is used for eliminating "noisy" observations. A time series model that has components of seasonality, trend, and break estimates surface reflectance and brightness temperature. The time series model is updated dynamically with newly acquired observations. Due to the differences in spectral response for various kinds of land cover change, the CCDC algorithm uses a threshold derived from all seven Landsat bands. When the difference between observed and predicted images exceeds a threshold three consecutive times, a pixel is identified as land surface change. Land cover classification is done after change detection. Coefficients from the time series models and the Root Mean Square Error (RMSE) from model estimation are used as input to the Random Forest Classifier (RFC). We applied the CCDC algorithm to one Landsat scene in New England (WRS Path 12 and Row 31). All available (a total of 519) Landsat images acquired between 1982 and 2011 were used. A random stratified sample design was used for assessing the change detection accuracy, with 250 pixels selected within areas of persistent land cover and 250 pixels selected within areas of change identified by the CCDC algorithm. The accuracy assessment shows that CCDC results were accurate for detecting land surface change, with producer's accuracy of 98% and user's accuracies of 86% in the spatial domain and temporal accuracy of 80%. Land cover reference data were used as the basis for assessing the accuracy of the land cover classification. The land cover map with 16 categories resulting from the CCDC algorithm had an overall accuracy of 90%.

© 2014 Elsevier Inc. All rights reserved.

1. Introduction

Mapping and monitoring land cover have been widely recognized as an important scientific goal (Anderson, 1976; Foody, 2002; Friedl et al., 2002; Hansen, Defries, Townshend, & Sohlberg, 2000; Homer, Huang, Yang, Wylie, & Coan, 2004; Loveland et al., 2000; Wulder et al., 2008). Land cover influences the energy balance, carbon budget, and hydrological cycle as many different physical characteristics change as a function of land cover, such as albedo, emissivity, roughness, photosynthetic capacity, and transpiration. Land cover change can be natural or anthropogenic, but with human activity increasing, the Earth surface has been modified significantly in recent years by various kinds of land cover change. Knowledge of land cover and land cover change is necessary for modeling the climate and biogeochemistry of the Earth system and for many kinds of management purposes. Satellite images have long been used to assess the Earth surface because of repeated synoptic collection of consistent measurements (Lambin & Strahler, 1994).

1.1. Monitoring land cover change with remote sensing

Images from the Landsat series of satellites are one of the most important sources of data for studying different kinds of land cover change, such as deforestation, agriculture expansion and intensification, urban growth, and wetland loss (Coppin & Bauer, 1996; Galford et al., 2008; Jensen, Rutchey, Koch, & Narumalani, 1995; Seto et al., 2002; Woodcock, Macomber, Pax-Lenney, & Cohen, 2001), due to their long record of continuous measurement, spatial resolution, and near nadir observations (Pflugmacher, Cohen, & Kennedy, 2012; Woodcock & Strahler, 1987; Wulder et al., 2008). One of the drawbacks of Landsat data is the relatively low temporal frequency. For each Landsat sensor, overpasses of the same location occur every 16 days, and data at this temporal frequency are only common within the United States where the sensors are turned on for every overpass. For other parts of the world, the frequency of data collection is generally less, depending on many factors such as cloud cover predictions and availability of international ground stations (Arvidson, Goward, Gasch, & Williams, 2006). Even for images that are collected, clouds reduce the amount of usable data (Zhang, Rossow, Lacis, Oinas, & Mishchenko, 2004). Therefore, most change detection algorithms using Landsat have used two dates of Landsat images (Collins & Woodcock, 1996; Coppin, Jonckheere, Nackaerts, Muys,

---

* Corresponding author. Tel.: +1 617 233 6031.
  E-mail address: zhuzhe@bu.edu (Z. Zhu).

& Lambin, 2004; Healey, Cohen, Yang, & Krankina, 2005; Masek et al., 2008; Singh, 1989). Though these kinds of algorithms are relatively simple to implement, they are not always applicable. It may take a few years to find an ideal pair of Landsat images that are free of clouds, cloud shadows, and snow (hereafter referred to as "clear") and acquired at the same time of year.

To find change over shorter time intervals, several new change detection algorithms using many dates of Landsat images (typically one image per year) are appearing in the literature (Goodwin et al., 2008; Hostert, Röder, & Hill, 2003; Huang et al., 2010; Kennedy, Cohen, & Schroeder, 2007; Vogelmann, Tolk, & Zhu, 2009). However, these newly developed algorithms still have limitations related to selection of ideal Landsat images. For example, to minimize the influences of phenology and sun angle differences, the ideal images should fall within the same season. Moreover, though they can use images that are partly covered by clouds, they still need most of the images to be cloud-free. To satisfy all these requirements, the best these algorithms can typically provide is annual or biennial change results (Huang et al., 2010; Kennedy et al., 2007).

Recently, Moderate Resolution Imaging Spectroradiometer (MODIS) time series data have been explored for monitoring various kinds of land cover change (Eklundh, Johansson, & Solberg, 2009; Galford et al., 2008; Jin & Sader, 2005; Lunetta, Knight, Ediriwickrema, Lyon, & Worthy, 2006; Roy, Jin, Lewis, & Justice, 2005; Verbesselt, Hyndman, Newnham, & Culvenor, 2010; Xin, Olofsson, Zhu, Tan, & Woodcock, 2012), because of its higher temporal frequency. The coarse spatial resolution of the MODIS data limits its ability for detecting small changes (Jin & Sader, 2005), which is common for anthropogenic changes. Also, issues of Bidirectional Reflectance Distribution Function (BRDF) effects (Schaaf et al., 2002), large differences in the projected Instantaneous Field of View (IFOV) (Xin et al., 2012), and gridding artifacts (Tan et al., 2006) make comparison of multitemporal MODIS images difficult. To monitor changes as they are occurring and to be able to identify changes small in size, the remote sensing community needs an algorithm that uses fine spatial resolution data such as Landsat and uses as many observations as possible to detect land cover change accurately and quickly.

1.2. Land cover classification

Land cover classification is one of the most studied topics in remote sensing, and land cover maps provide the basis for many applications like modeling of carbon budgets, management of forests, and estimation of crop yield (Jung, Henkel, Herold, & Churkina, 2006; Lark & Stafford, 1997; Rogan et al., 2010; Wolter, Mladenoft, & Crow, 1995). While it is relatively easy to generate a land cover map from remotely sensed data, it is not easy to make it accurate. Using multitemporal images as inputs is reported to help improve classification accuracy (Carrao, Goncalves, & Caetano, 2008; Guerschman, Paruelo, Bella, Giallorenzi, & Pacin, 2003; Wolter et al., 1995; Zhu, Woodcock, Rogan, & Kellndorfer, 2012), especially for vegetation, because of the unique phenological characteristics of different vegetation types. To achieve higher classification accuracy, most current land cover products are generated using multitemporal images as their inputs (Friedl et al., 2010; Gopal, Woodcock, & Strahler, 1999; Hansen et al., 2000; Homer et al., 2004; Loveland et al., 2000; Tucker, Townshend, & Goff, 1985).

The use of multitemporal images also can cause problems for conventional automated classification algorithms. First, they need all dates of images to be free of clouds to classify every pixel in the image, which is often not possible, especially for sensors with relatively low temporal frequency like Landsat. For some cloudy locations, it may be necessary to wait a few years to get multiple Landsat images in the same year without clouds and snow. Therefore, most Landsat-based land cover maps are produced at the interval of five or ten years, which greatly reduces their "currency". Second, when making land cover maps with multitemporal images, we typically assume there is

no land cover change in the time interval between the different images. This assumption is not always valid, especially when images from long time intervals are used, or for areas that are changing frequently (Rogan, Franklin, & Roberts, 2002). Moreover, the land cover maps produced from conventional methods cannot be used directly for identifying land cover change because frequently the magnitude of the error in classification is much larger than the amount of land cover change (Friedl et al., 2010; Fuller, Smith, & Devereux, 2003). If we compare land cover maps produced at different times for detecting change, the errors from the classification process will show up as change and this causes serious problems for places where the sizes of changes are small. Therefore, the remote sensing community needs a classification algorithm that: (1) increases the time period over which land cover maps remain "current"; (2) works for areas where multiple kinds of land cover change is common, and (3) makes land cover maps comparable between times for identification of change.

1.3. Introduction to the CCDC algorithm

The opening of the Landsat archive in 2008 (Woodcock et al., 2008) has led to big changes in the way Landsat images are being used. Previously, a single Landsat image would cost hundreds of U.S. dollars. To minimize costs, most researchers typically chose to use only a few cloud-free Landsat images acquired during the growing season for analysis. Following free access to the Landsat archive, studies using lots of Landsat images are appearing (Brooks, Thomas, Wynne, & Coulston, 2012; Goodwin et al., 2008; Hansen et al., 2013; Huang et al., 2010; Kennedy, Yang, & Cohen, 2010; Melaas, Friedl, & Zhu, 2013; Vogelmann et al., 2009; Zhu, Woodcock, & Olofsson, 2012). In this paper, we seek to improve monitoring of land cover and land cover change for a region in coastal New England by developing an approach that uses all available Landsat data. We use all available Landsat data because there are many clear observations in Landsat images that have a high percentage of clouds. Fig. 1 is a cumulative histogram of the percentage of clear observations in Landsat images as it relates to cloud cover. The cloud cover estimates are derived from a newly developed Fmask algorithm (Zhu & Woodcock, 2012) for Path 12 Row 31 between 1982 and 2011. Based on this information, if we only use Landsat images with cloud cover less than 10%, as has been common in the past, we would omit more than 50% of the total clear observations. Even Landsat images with more than 40% cloud cover contain almost 20% of the total clear observations. The use of all available Landsat data has opened a door for many studies that could not be imagined before, such as the study of phenology at Landsat scales (Melaas et al., 2013) or detection of forest disturbance continuously at high
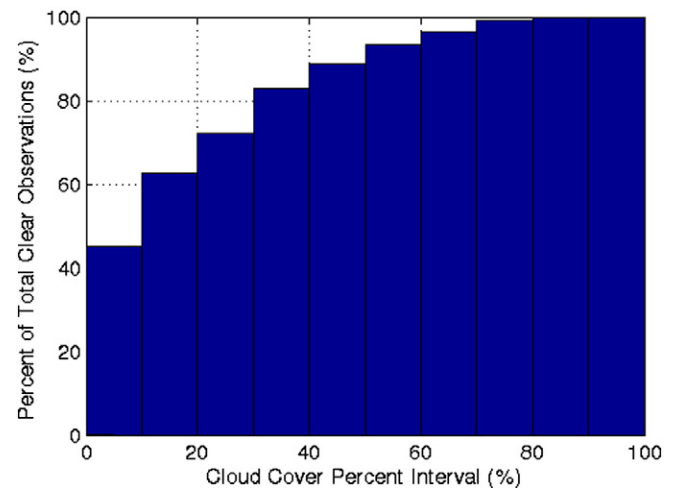

Fig. 1. Percent of total clear observations vs. cloud cover percent interval based on all available Landsat TM/ETM+ images from 1982 to 2011 for Path 12 Row 31 (New England).

spatial resolution and high temporal frequency (Zhu, Woodcock, & Olofsson, 2012).

Using all available TM/ETM+ observations from Landsat 4, 5, and 7, we developed a new Continuous Change Detection and Classification (CCDC) algorithm that helps minimize the issues that undermine the more conventional change detection and classification methods mentioned above. The use of the term "continuous" here refers to the capability to detect change detection every time a new image is collected. If it is updated as new images are collected, then the approach begins to approach near real-time change detection. The use of "continuous" in the name of the algorithm also follows from the idea that a land cover map can be produced for any given time within the time period covered by images. One additional note is that this new algorithm is able to detect many kinds of land cover change.

2. Data and study area

2.1. Study area

The study area is located in coastal New England, United States (Fig. 2). It includes all of Rhode Island, as well as much of Eastern Massachusetts and parts of Eastern Connecticut. It has been selected because: (1) it includes Boston making field visits easy; (2) it includes a wide variety of environments and land covers that provide examples of many of the primary kinds of land cover change occurring in the United States, including: extensive urbanization (three major metropolitan areas—Boston, Providence, and Worcester), abandonment of

agricultural fields, and forest clearing; and (3) it is rare to find a cloud-free Landsat image in this study area, making it an outstanding place to test the robustness of this new algorithm.

2.2. Landsat data

All available Level 1 Terrain (corrected) (L1T) Landsat TM/ETM+ images for Worldwide Reference System (WRS) Path 12 and Row 31 with cloud cover less than 80% (based on the Fmask results) were used (Fig. 2). A total of 519 images from Landsat 4 TM (3 images), Landsat 5 TM (331 images), and Landsat 7 ETM+ (185 images) between 1982 and 2011 were used. The images are fairly evenly distributed throughout the year (Table 1), the months during the growing season (July, August, and September) having slightly more images than the other months.

2.3. Land cover reference data

Land cover reference data collected at any given time (within the time period covered by the Landsat images) will work for training the CCDC algorithm. The land cover reference data used in this paper were previously used to calibrate the HERO Massachusetts Forest Monitoring Program (MaFoMP) 2000 land cover product (Rogan et al., 2010). They were created with the aid of aerial photographs and many field visits between 2005 and 2007. All reference sites were 60 × 60 m in dimension, and were distributed throughout Massachusetts to capture the variability in reflectance values within the study area. In the original
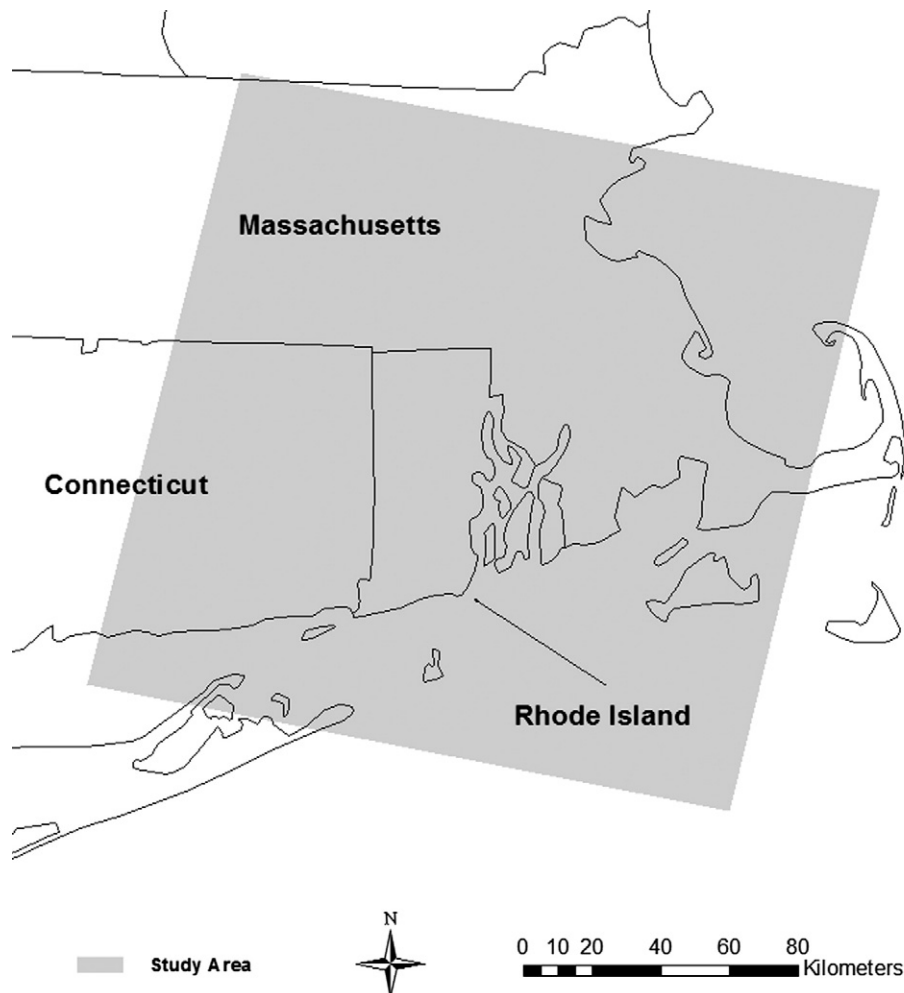

Fig. 2. Study area for testing the CCDC algorithm.

Table 1
Frequency by month of all available Landsat data for the study area at Path 12 Row 31.

Month	Jan.	Feb.	Mar.	Apr.	May	Jun.	Jul.	Aug.	Sept.	Oct.	Nov.	Dec.
Number of images	41	41	40	41	43	43	52	48	52	47	40	31

data, *water* is divided into two land cover classes (*shallow water* and *deep water*). To simplify, we combined *shallow water* and *deep water* into one land cover class—*water*. There are a total of 8220 reference sites for 16 categories of land cover (Table 2).

3. Methods

This study is a "prototype" for continuous change detection and classification using all available Landsat data. Testing this approach for other regions with different environments will be a future research direction. This CCDC algorithm has several components, including: image preprocessing, continuous change detection, and continuous land cover classification.

3.1. Image preprocessing

3.1.1. Atmosphere correction
Geometric registration and atmospheric correction are critical to the CCDC algorithm, as they facilitate comparison of images through time. In this research, we only use Landsat L1T images as they are more precisely registered than the Level 1 Systematic (corrected) (L1G) images. Atmospheric correction is performed using the Landsat Ecosystem Disturbance Adaptive Processing System (LEDAPS) atmospheric correction tool (Masek et al., 2006; Vermote et al., 1997), in which the raw DN values are converted into Surface Reflectance (SR) and Brightness Temperature (BT).

3.1.2. Screening of cloud, cloud shadow, and snow
Clouds, cloud shadows, and snow were initially masked using a newly developed object-based algorithm called Fmask (Zhu & Woodcock, 2012). Though the Fmask algorithm provides relatively accurate masks for clouds, cloud shadows, and snow, it is not perfect. Moreover, there are other ephemeral changes such as thick aerosols, smoke, or flooding that may also get confused with land cover change. Therefore, the CCDC algorithm uses a second step to further screen outliers previously missed by the Fmask algorithm based on multitemporal analysis of the Landsat data (Zhu & Woodcock, in preparation; Zhu, Woodcock, & Olofsson, 2012). This approach first estimates a time series model based on the "clear" observations previously identified by Fmask and then detects outliers by comparing model estimates and Landsat observations. The Robust Iteratively Reweighted Least Squares (RIRLS)

method (DuMouchel & O'Brien, 1989; Holland & Welsch, 1977; O'Leary, 1990; Street, Carroll, & Ruppert, 1988) is used for estimating the time series model (Eq. 1). The robust feature of the RIRLS method reduces the influence of ephemeral changes, or pixels affected by clouds, shadows, or snow that were not identified by Fmask.

$$\hat{\rho}(i,x)_{RIRLS} = a_{0,i} + a_{1,i}\cos\left(\frac{2\pi}{T}x\right) + b_{1,i}\sin\left(\frac{2\pi}{T}x\right) + a_{2,i}\cos\left(\frac{2\pi}{NT}x\right) + b_{2,i}\sin\left(\frac{2\pi}{NT}x\right)$$

(1)

where,

x	Julian date
I	the ith Landsat Band
T	number of days per year (T = 365)
N	number of years of Landsat data
$a_{0,i}$	coefficient for overall values for the ith Landsat Band
$a_{1,i},b_{1,i}$	coefficients for intra-annual change for the ith Landsat Band
$a_{2,i},b_{2,i}$	coefficients for inter-annual change for the ith Landsat Band
$\hat{\rho}(i,x)_{RIRLS}$	predicted value for the ith Landsat Band at Julian date x based on RIRLS fitting.

Due to the fact that clouds and snow make Band 2 brighter and cloud shadows and snow make Band 5 darker, we estimate time series models for Band 2 and Band 5. By comparing the actual Landsat observations and the corresponding model predictions, it is comparatively easy to identify any remaining clouds, cloud shadows, snow, and other ephemeral changes (Fig. 3). If any of the conditions in Eq. (2) are met, this observation is identified as an outlier and removed from further analysis.

The model estimation starts when there are a total of 15 "clear" determined by Fmask) observations. The first 12 are compared between observed and model predicted values to decide whether there are outliers. The reason for picking the first 12 clear observations is that the time series model of the CCDC algorithm has 4 coefficients (see Section 3.2 for detail) and 12 clear observations (three times the number of coefficients) help make model estimation robust and accurate. We do not perform the multitemporal cloud, cloud shadow, and snow screening algorithm for the last 3 clear observations because the CCDC algorithm needs extra observations at the end of the time series to

Table 2
16-categories land cover description.

Class	Number of sites	Description
Orchards	234	Managed plantation of fruit trees, primarily apples
Cranberry Bogs	265	Managed bog containing cranberry bushes, seasonally flooded
Pasture/Row Crops	541	Open and cultivated agricultural grasslands
Deciduous Forest	570	Forested land ≥80% broadleaved deciduous canopy cover
Conifer Forest	582	Forested land ≥80% needleleaved evergreen canopy cover
Mixed Forest	702	Forest land >20% conifer and <80% deciduous canopy cover
Golf Course	486	Highly managed open grasslands
Grassland	502	Grassland dominated open spaces
Low Density Residential	511	Residential land with equal parts impervious surface & vegetation
High Density Residential	466	Residential land minimally vegetated, >60% impervious surface
Commercial/Industrial	613	Impervious surface
Water	1088	Standing water present >11 months
Wetland	513	Vegetated lands with a high water table
Salt Marsh	436	Tidal saltwater rivers/mudflats & surrounding herbaceous cover
Sand Quarry	374	Sand & gravel mining pits
Bare Soil	337	Bare land sparsely vegetated, >60% soil background

allow the model to respond to land surface change so that changes that occur at the end of the initial model estimation will not be identified as outliers. The reason for picking 3 clear observations is that the CCDC algorithm uses three consecutive observations to determine if a pixel is changed or not (see Section 3.3 for detail) and three clear observations are enough for the time series model to respond to land surface change. If any of the first 12 pixels are found to be possible cloud, cloud shadow, snow or other ephemeral changes, it is removed from the clear pixel list. Due to computational limitations

and the requirement of continuous monitoring, the CCDC algorithm only applies this multitemporal cloud, cloud shadow, and snow detection algorithm during the time of model initialization (see Section 3.2 for detail). For observations acquired after model initialization, only the Fmask algorithm is used.

$$\rho(2,x) - \hat{\rho}(2,x)_{RIRLS} > 0.04 \ \ OR \ \ \rho(5,x) - \hat{\rho}(5,x)_{RIRLS} < -0.04 \qquad (2)$$

where,

x	Julian date
$\rho(i,x)$	Observed value for the ith Landsat Band at Julian date x.
$\hat{\rho}(i,x)_{RIRLS}$	Predicted value for the ith Landsat Band at Julian date x based on RIRLS fitting (Eq. 1).

3.2. The CCDC time series model

Generally, land surface change can be divided into three categories: (1) intra-annual change (Fig. 4A), caused by vegetation phenology driven by seasonal patterns of environmental factors like temperature and precipitation; (2) gradual inter-annual change (Fig. 4B), caused
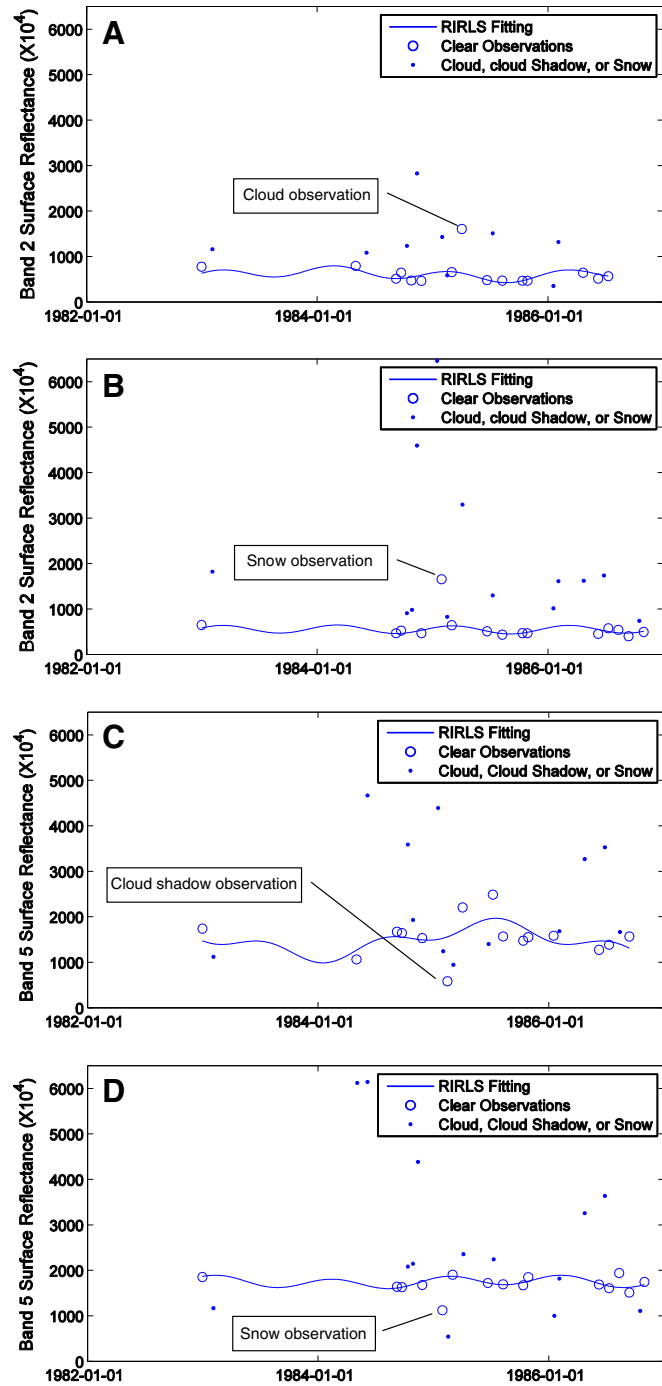

Fig. 3. Illustration of multitemporal screening of cloud, cloud shadow, and snow. The circles are pixels identified as "clear" by Fmask and those labeled are the ones found by the multitemporal analysis to be clouds, cloud shadows, or snow. Because clouds and snow make Band 2 brighter (Fig. 3A & B) while cloud shadows and snow make Band 5 darker (Fig. 3C & D), clouds, cloud shadows, and snow are easily identified by comparing the actual Landsat observations with the model predictions.
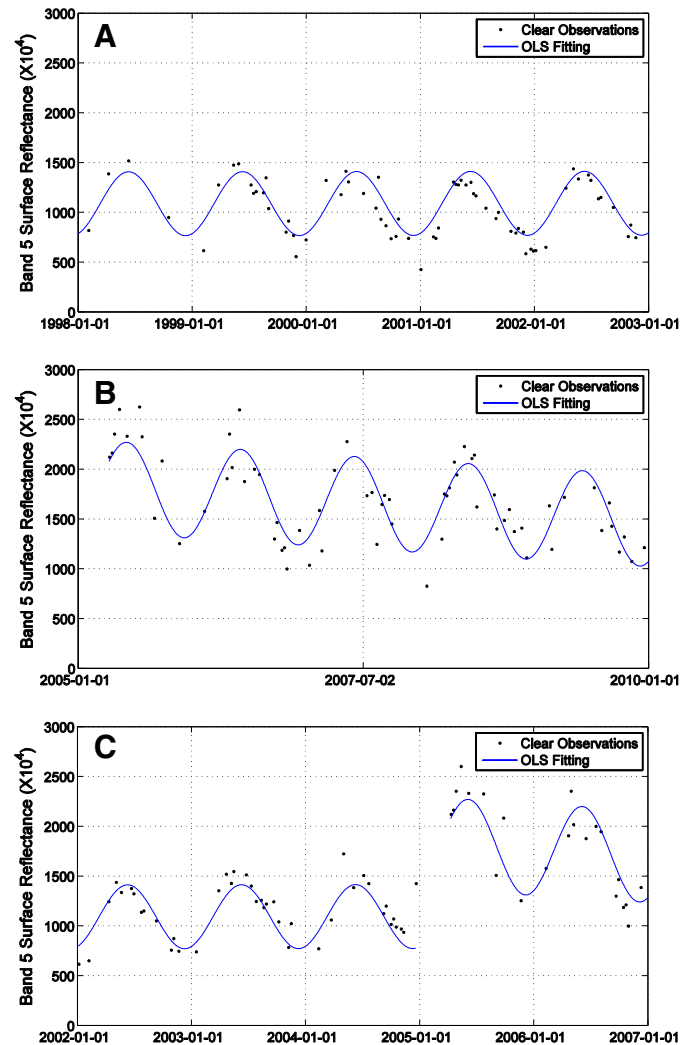

Fig. 4. Three categories of land surface change shown in Band 5 surface reflectance: (1) intra-annual change (or seasonality) (Fig. 4A); (2) inter-annual change (or trend) (Fig. 4B); and (3) abrupt change (or break) (Fig. 4C).

by climate variability, vegetation growth or gradual change in land management or land degradation; and (3) abrupt change (Fig. 4C), caused by deforestation, floods, fire, insects, urbanization and so on. Therefore, we use a time series model that has components of seasonality, trend, and breaks that captures all three categories of surface change (Eq. 3). The model coefficients are estimated by the Ordinary Least Squares (OLS) method based on the remaining clear Landsat observations. We use OLS instead of RIRLS simply because it is faster and more accurate when all the significant outliers have been excluded.

$$\hat{\rho}(i, x)_{OLS} = a_{0,i} + a_{1,i} \cos\left(\frac{2\pi}{T}x\right) + b_{1,i} \sin\left(\frac{2\pi}{T}x\right) + c_{1,i}x \qquad (3)$$

$$\{\tau_{k-1}^* < x \leq \tau_k^*\}$$

where,

x	Julian date
i	the ith Landsat Band
T	number of days per year (T = 365)
$a_{0,i}$	coefficient for overall value for the ith Landsat Band
$a_{1,i}, b_{1,i}$	coefficients for intra-annual change for the ith Landsat Band
$c_{1,i}$	coefficient for inter-annual change for the ith Landsat Band
τ_k^*	the kth break points.
$\hat{\rho}(i, x)_{OLS}$	predicted value for the ith Landsat Band at Julian date x.

In the time series model, the overall value, or mean, for the ith Landsat Band is captured by $a_{0,i}$. Coefficients $a_{1,i}$ and $b_{1,i}$ are used to estimate the intra-annual changes caused by phenology and sun angle differences for the ith Landsat Band. The inter-annual change for the ith Landsat Band is captured by $c_{1,i}$. Ideally, the more the coefficients included, the more accurate the model will be. However, when there are too many coefficients, the model may start to fit to noise. Fig. 5 shows the results of the model for the different components of the time series model. If we only use a single constant coefficient ($a_{0,i}$), it can only capture the overall reflectance and all the intra- and inter-annual variability is lost (Fig. 5A). By adding the inter-annual trend ($c_{1,i}$), the time series model is able to capture the trends, however, losing all intra-annual variability (Fig. 5B). The best result comes when all three components are included (Fig. 5C).

3.3. Continuous change detection

The basis of our method is comparison of model predictions with clear satellite observations to find change. Ideally, a single date comparison would be definitive for detecting change. However, there is sufficient noise in the system due to factors like undetected clouds, cloud shadows, snow, atmospheric haze, smoke, and changes in soil wetness that will lead to numerous false positive errors in change detection when using a single date for comparison (Zhu, Woodcock, & Olofsson, 2012). While noise factors tend to be ephemeral in nature, land cover change is more persistent through time. The CCDC algorithm minimizes ephemeral effects by processing a set of dates together as a group for identifying land cover change. That is, if a pixel is observed to change in multiple consecutive images, it is more likely to be land cover change. Based on previous studies (Zhu, Woodcock, & Olofsson, 2012), change identified in three successive dates showed the best results. Therefore, pixels showing change for one or two consecutive times will be flagged as "possible change" and if a third consecutive change is found, the pixel is assigned to the "change" class.

To detect one kind of land cover change such as forest change, a single change index with a fixed threshold is sufficient (Zhu, Woodcock, & Olofsson, 2012). To find many kinds of land cover change, we need to use more spectral bands, as land cover change that is obvious in one
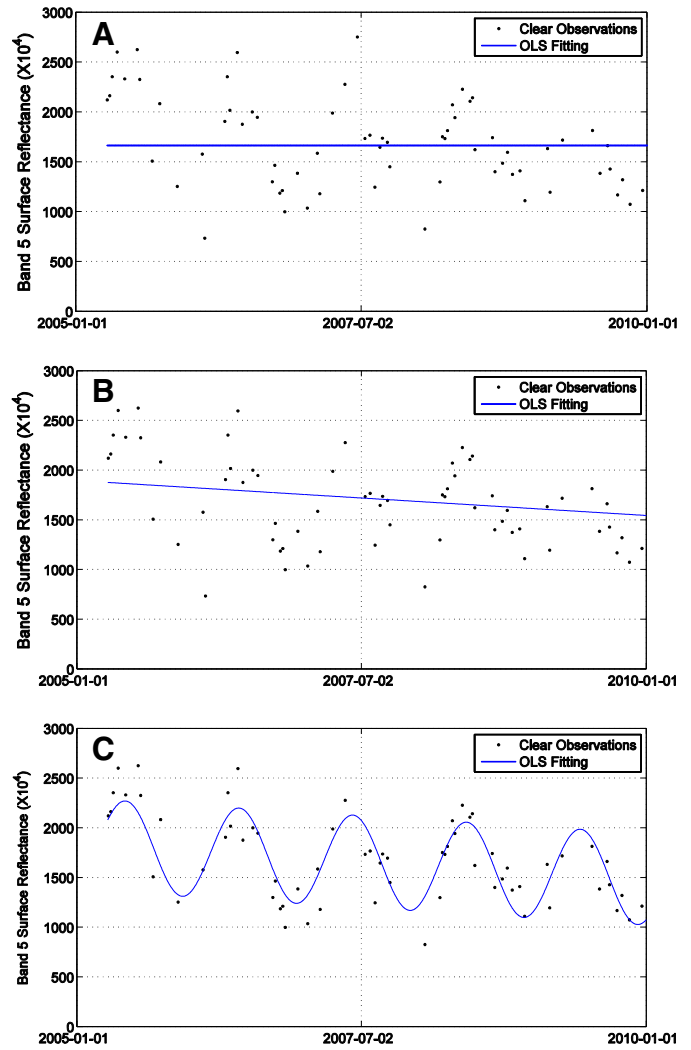

Fig. 5. Illustration of the OLS fitting results by including different components of the time series model. Fig. 5A shows the results when only including a single constant. Fig. 5B shows the results of using a constant and an inter-annual trend in the time series model. Fig. 5C shows the results of using all three components.

spectral band (or index), maybe difficult to identify in other spectral bands (or indices). Moreover, the threshold for defining change may also be different for different kinds of land cover change. Therefore, the CCDC algorithm uses all Landsat spectral bands and a data-driven threshold (adjusted for each individual pixel) to detect many kinds of land cover change. The OLS method (Eq. 3) is applied to all seven Landsat bands and the RMSE is computed for each spectral band. The difference between observations and model predictions for each Landsat band is normalized by three times the RMSE. We use three times the RMSE due to the fact that the spectral signals usually deviate from model prediction by more than three times the RMSE when land cover change occurs. Fig. 6 illustrates how the "three times the RMSE" criterion is used for detecting land cover change for a deforestation pixel. When there is no land cover change, the next three clear observations are always within the model predicted ranges ($\pm 3 \times RMSE$) (Fig. 6A & C). Fig. 6B shows how change is initially detected by comparing the next three consecutive clear observations with model predictions. Fig. 6 only uses one Landsat band (Band 5) to illustrate the algorithm, but all seven spectral bands are used to detect change. In Fig. 7, the same deforestation pixel as Fig. 6 is shown and when deforestation occurred, all spectral bands changed significantly. Therefore, the
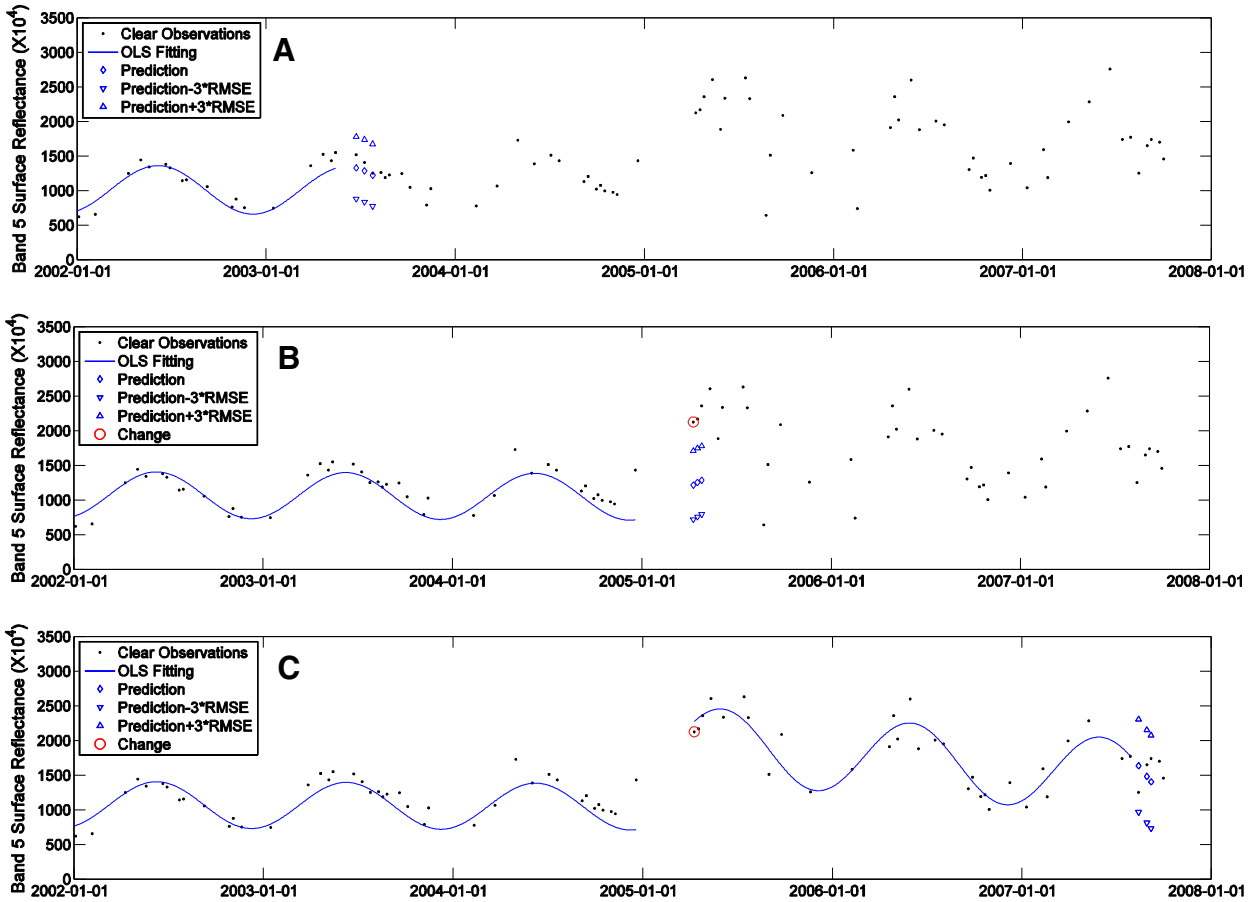
Fig. 6. This figure illustrates the reason for using the threshold of three times the RMSE for continuous change detection. Fig. 6A shows the model prediction and three times the RMSE before change occurred. Fig. 6B shows the model prediction and three times the RMSE when change occurred. Fig. 6C shows the model prediction and three times the RMSE after change occurred.

CCDC algorithm averages the difference between observations and model predictions that have been normalized by three times the RMSE for all seven Landsat bands, and if the result is larger than 1 for three consecutive clear observations, a change is identified (Eq. 4). Otherwise, if the values for only one or two consecutive observations are larger than 1, it will be regarded as an ephemeral change and the observations will be flagged as outliers. The CCDC algorithm updates the time series model when new clear observations become available, adding a dynamic character to the process that allows the time series to adjust over time. Eq. (4) provides the details of the land cover change algorithm. Note that the continuous change detection algorithm assumes that the phenology is consistent for stable land covers, which may not be true for some semi-arid environments due to the variation of the inter-annual differences. Further studies may be necessary if we want to expand the use of this algorithm to other parts of the world.

$$\frac{1}{k}\sum_{i=1}^{k}\frac{|\rho(i,x)-\hat{\rho}(i,x)_{OLS}|}{3\times RMSE_i}>1 \ (\text{three times consecutively}) \qquad (4)$$

where,

x	Julian date
i	the ith Landsat band
k	the number of Landsat bands
$\rho(i,x)$	observed value for the ith Landsat Band at Julian date x

$\hat{\rho}(i,x)_{OLS}$　predicted value for the ith Landsat Band at Julian date x based on OLS fitting (Eq. 3).

Land cover change that occurs within the time of model initialization (start of the model estimation) can bias the time series model predictions. Therefore, if there is land cover change during the process of model initialization, the CCDC algorithm will remove the first clear observation and add one more clear observation and this process will continue until no possible change is detected within the initialization time period. As a result, each pixel will have its own start date for model initialization and this also leads to different start dates for the continuous change detection and classification process. Three approaches are used to detect change that might have occurred during the time period covered by the first 12 clear observations used for model initialization: abnormal slope, abnormal first observation, and abnormal last observation.

For pixels of stable land cover, the magnitude of the slope of the time series model will be relatively small. If land cover change occurs during the time of model initialization (t_{model}), the observation will usually deviate more than three times the RMSE, making the slope of the time series model larger than $3 \times RMSE_i/t_{model}$. Therefore, the slope of the time series model for the ith Band is normalized by $3 \times RMSE_i/t_{model}$ (see Eq. 5 for details), and if the average value of the normalized slope for all bands is larger than 1, it will be detected as an abnormal slope, indicating a possible change within the model initialization time. On the other hand, if land cover change occurs at the start or the end of model initialization, there may not be enough observations affected by

the land cover change to significantly influence the magnitude of the slope, but they may still influence model estimation. In this case, the CCDC algorithm compares Landsat observations with model predictions for the first and the last observations during model initialization. As a few change observations at the very beginning or end of the model initialization period will not influence model prediction significantly, they

can still be detected by comparing observations with model predictions. Therefore, the CCDC algorithm also calculates the difference between observations and model predictions for the first and the last observations. Next, the difference between observed and predicted values for each Landsat band is normalized by RMSEi (see Eq. 5 for details), and if the average value of the normalized difference for all Landsat bands
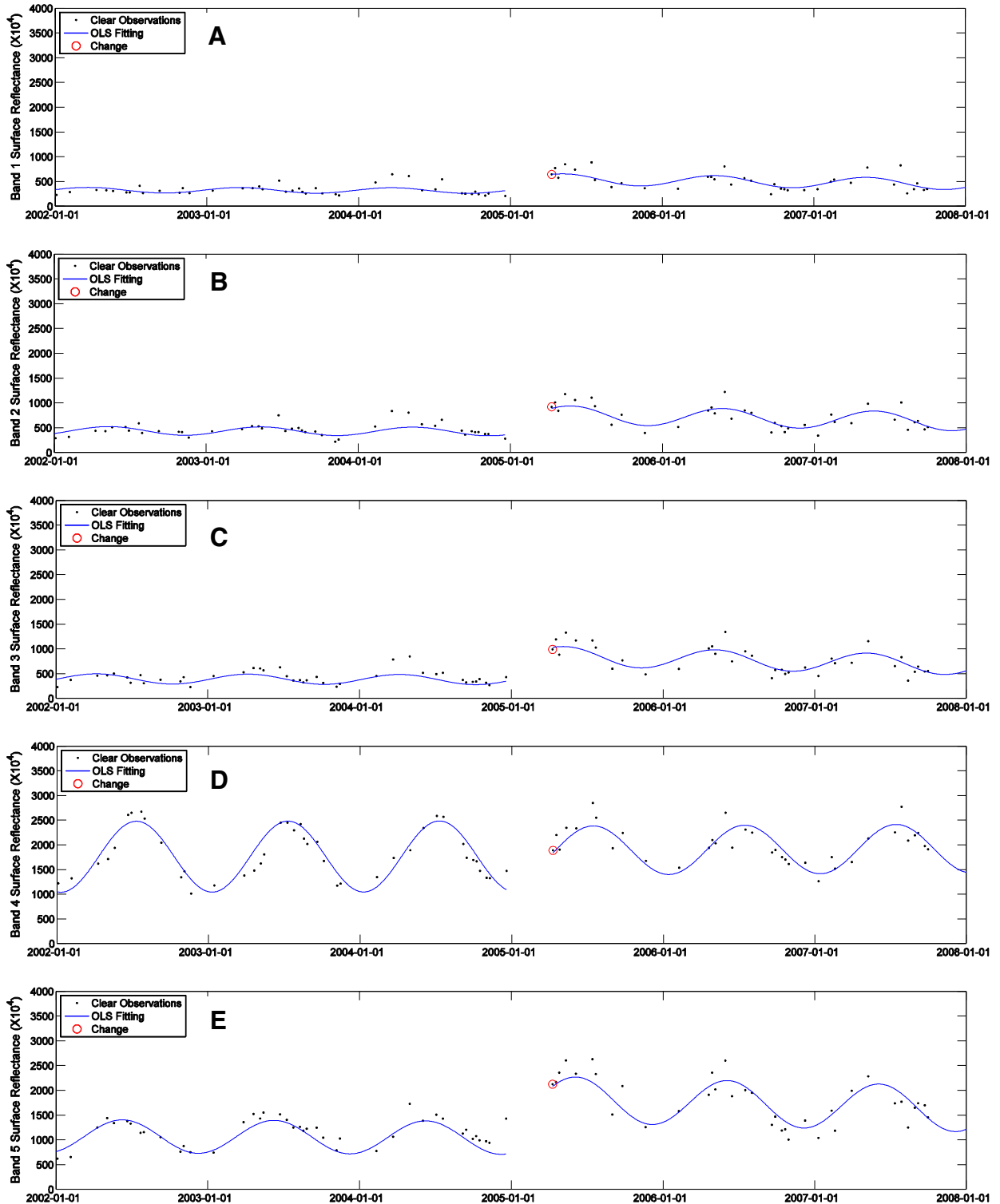

Fig. 7. This figure illustrates how the seven Landsat spectral bands (Bands 1–7) deviate from their original trajectories when deforestation occurred.
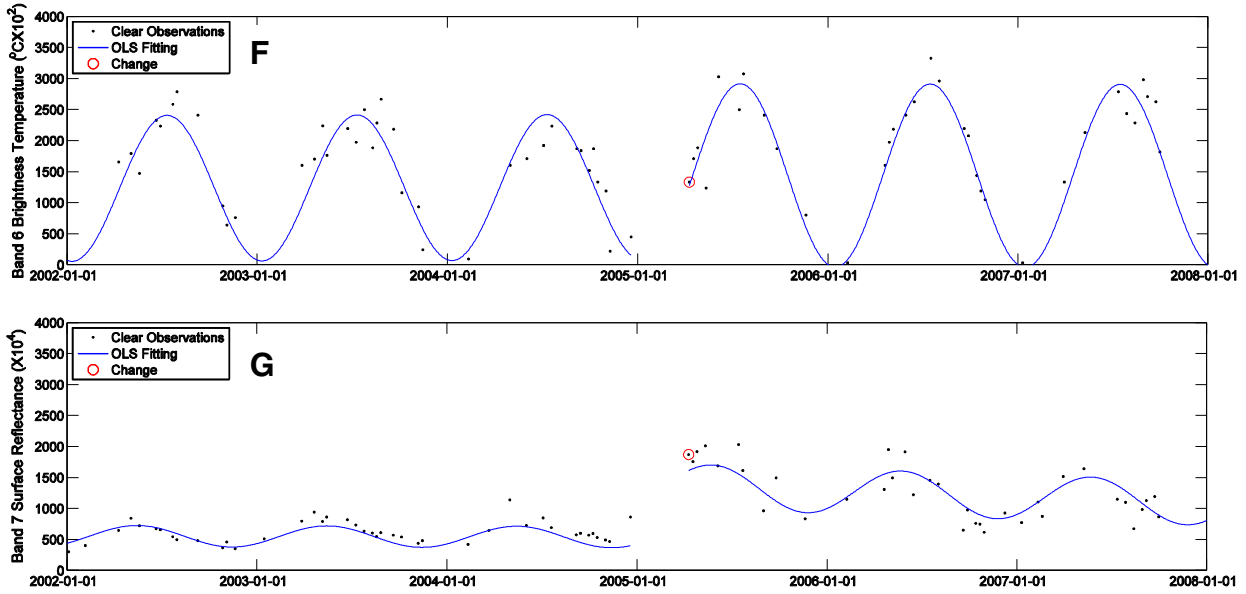
Fig. 7. (continued).

is larger than 1 for the first or the last observation, it will be identified as an abnormal observation, indicating possible change within the model initialization period. As soon as the model initialization is finished, it will be used as the basis for continuous change detection and classification.

$$\frac{1}{k}\sum_{i=1}^{k}\frac{|c_{1,i}(x)|}{3 \times RMSE_i/t_{model}}>1 \quad OR \quad \frac{1}{k}\sum_{i=1}^{k}\frac{|\rho(i,x_1)-\hat{\rho}(i,x_1)_{OLS}|}{3 \times RMSE_i}>1 \quad (5)$$

$$OR \quad \frac{1}{k}\sum_{i=1}^{k}\frac{|\rho(i,x_n)-\hat{\rho}(i,x_n)_{OLS}|}{3 \times RMSE_i}>1$$

where,

x Julian date
x_1 the Julian date for the first observation during model initialization
x_n the Julian date for the last observation during model initialization
i the ith Landsat Band
k the number of Landsat bands (k = 7)
$RMSEi$ Root Mean Square Error for the ith Landsat Band (Eq. 3)
T_{model} the total time used for model initialization
$C_{1,i}$ coefficient for inter-annual change for the ith Landsat Band (Eq. 3)
$\rho(i,x)$ observed value for the ith Landsat Band at Julian date x
$\hat{\rho}(i,x)_{OLS}$ predicted value for the ith Landsat Band at Julian date x based on OLS fitting (Eq. 3).

3.4. Continuous land cover classification

Finding land cover change is important, but it will be more beneficial if we know the land cover categories before and after change. Instead of classifying the original Landsat images as conventional methods would, the CCDC algorithm uses the coefficients of time series models as the inputs for land cover classification. After the change detection process, each pixel will have its own time series models before and after any changes. By classifying the time series model coefficients, this algorithm can provide a land cover type for the entire time period for each time series model. Time series observations from all seven Landsat bands (including the thermal band) were used for the land cover classification. In general, it is usually not recommended to include thermal data in land cover classification due to its sensitivity to substantially different physical phenomena. Including thermal data can cause more harm than good in land cover classification. However, the CCDC algorithm is able to use the multitemporal thermal data in the form of the coefficients for overall temperature, trend in temperature, and intra-annual variation in temperature. In this approach, most of the short-term variability in temperature is removed and the general patterns related to surface characteristics remain, and they prove useful for improving land cover classification.

The main idea of the land cover classification is that different land cover classes will have different shapes for the estimated time series models. Fig. 8 illustrates different estimated time series models for four different kinds of land cover change that occurred in the study area. Taking Fig. 8A for instance, by classifying the first time series model, the CCDC algorithm is capable of providing a land cover class (*forest*) for this pixel between 2001 and 2003. Similarly, the classification results of the second time series model provide the land cover class (*developed*) for this pixel between 2005 and 2006. The gaps in the middle of two models are classified as "*disturbed*" in the land cover maps, because the large variability in the data during the transition time prevents model initialization. Note that when *forest* is changed to *developed*, the time series models show completely different shapes, especially for Band 4 and Band 6 (Fig. 8A). The reduction of Band 4 reflectance is easy to understand: *forest* reflects strongly in Band 4 while *developed* areas do not. The increase in Band 6 is mostly due to reduced evapotranspiration and urban heat island effects when *forest* is converted to *developed*. When *forest* is changed to *barren* (Fig. 8B), the most significant changes are observed in Band 5 and Band 7, as *forest* is usually low in SWIR bands but *barren* always has high reflectance in these spectral bands. For a pixel that has undergone a change from *forest* to *grass* (Fig. 8C), there is not much difference in the time series models in the visible bands, but the SWIR and thermal bands are quite different. For the pixel that changed from *forest* to *agriculture* (Fig. 8D), the time series models of the NIR and SWIR bands show the biggest difference. These examples illustrate that the information contained in the time series model is helpful for land cover classification and by using the coefficients of the time series model it is possible to provide a single land cover class for the entire period when change is not specifically identified.
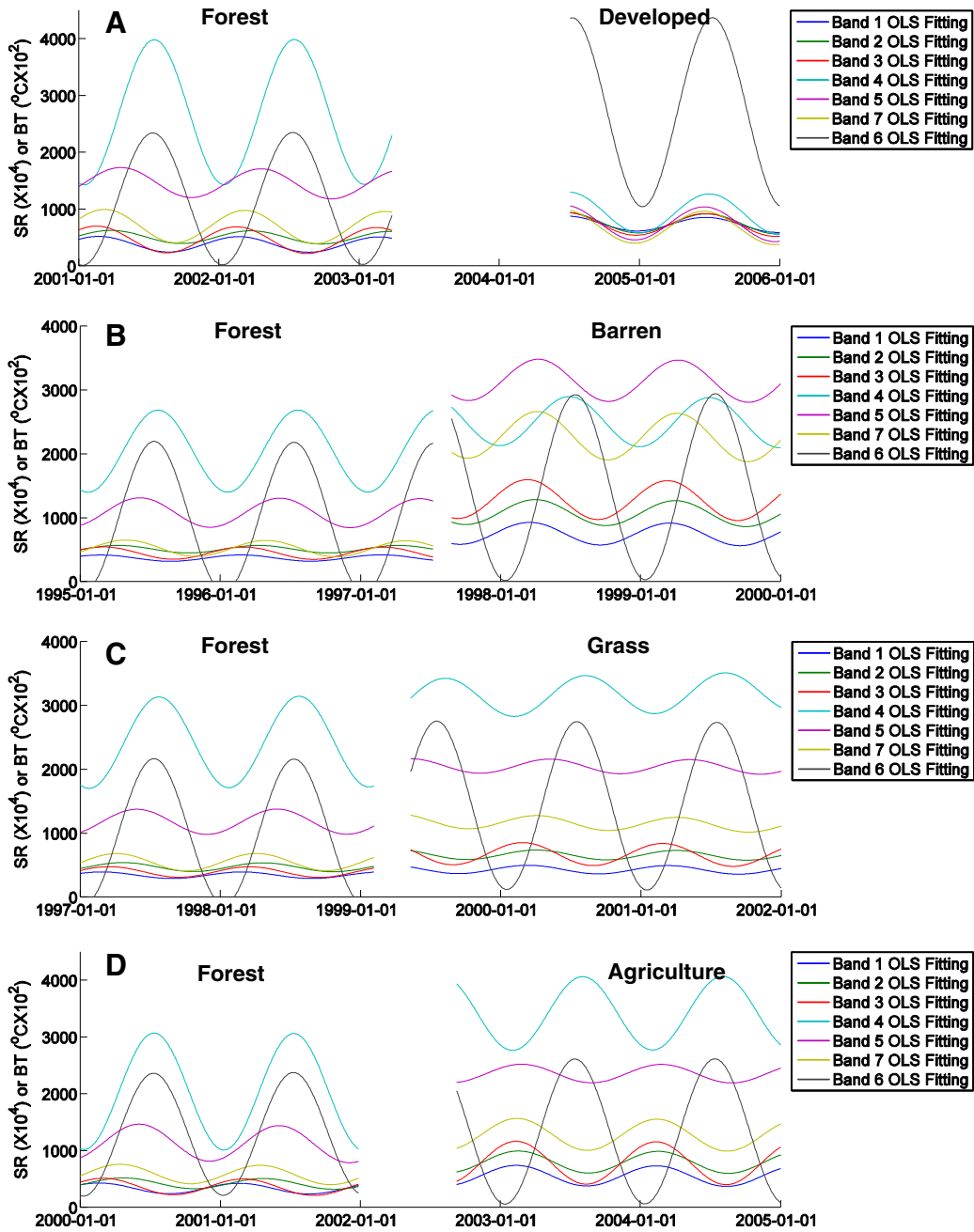
Fig. 8. Examples of the estimated time series models for all seven Landsat bands for the four most common land cover change in the study area.

Five variables ($\overline{\rho}, a_1, b_1, c_1$, and RMSE) generated from time series model estimation are used as inputs for land cover classification. The first variable ($\overline{\rho}$) represents the overall spectral value at the center of each time series model for each Landsat band. This overall value is calculated by adding a constant (a_0) and a slope (c_1) multiplied by the time to the middle of the time series model (Eq. 6). The second and the third variables (a_1 & b_1) provide temporal information about intra-annual (or season) patterns. The fourth variable (c_1) measures inter-annual differences or trends. The last variable (RMSE) is calculated during OLS fitting in Eq. (3) and measures how well the time series model fits the data. Fig. 9 shows the average from reference sites for the five different variables for different land cover categories. It is clear that different land covers show quite different shapes in the plots of the five variables, and this information is helpful for discriminating land cover types. Considering there are 7 spectral bands and each band has 5 variables, there are

35 variables used as the input for classification. As the reference data are collected between 2005 and 2007, the estimated coefficients of the reference pixels that were not detected to have land cover change between 2005 and 2007 are used for training the classifier. The Random Forest Classifier (RFC) is used to perform land cover classification because of its relatively high accuracy and computational efficiency (Breiman, 2001).

$$\overline{\rho}(i) = a_{0,i} + c_{1,i} \times \frac{t_{start} + t_{end}}{2}$$

(6)

where,

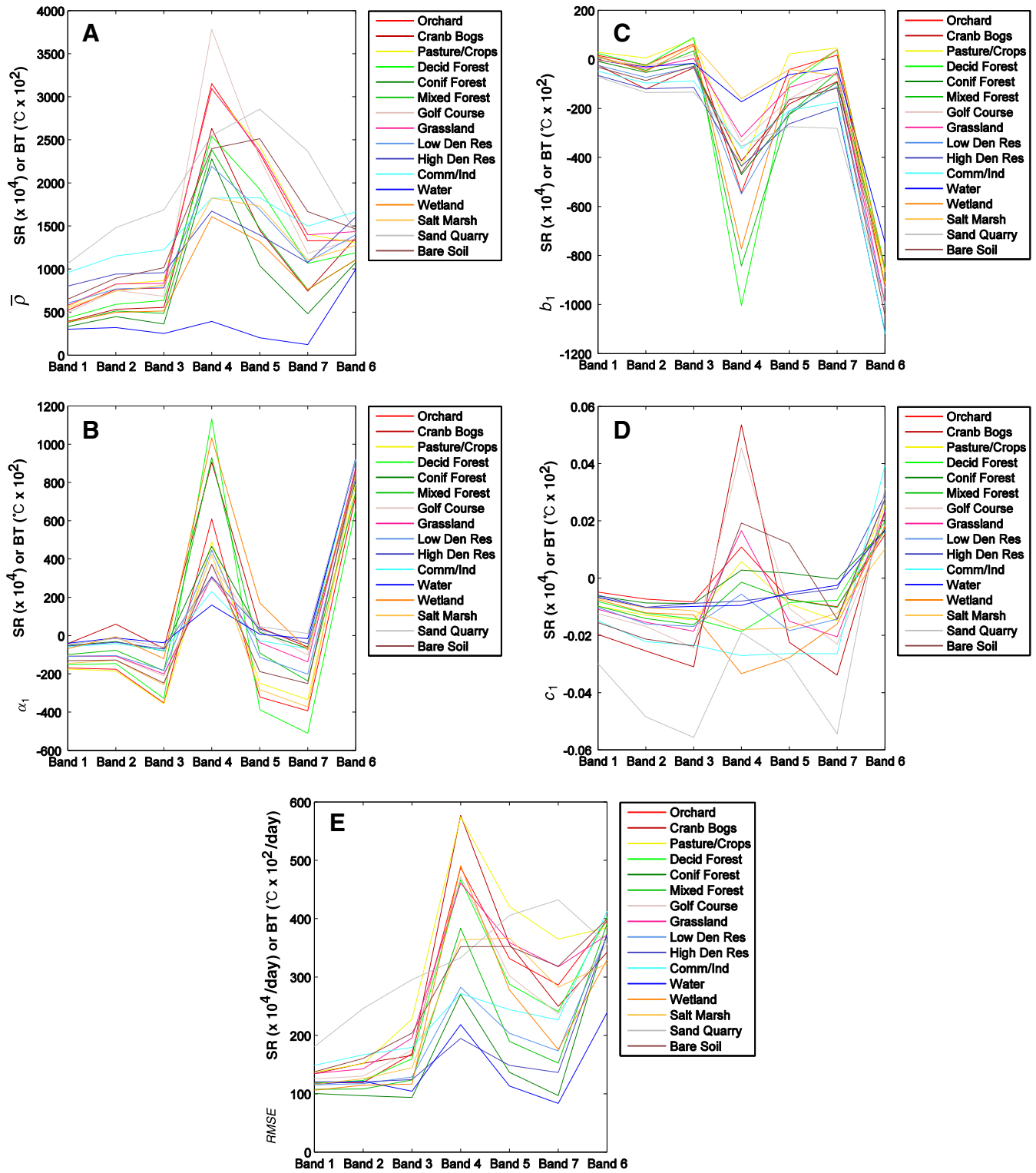|	
t_{start}	the time (Julian date) when model initialization starts
t_{end}	the time (Julian date) when model initialization ends

Fig. 9. The value of the five variables, $(\overline{\rho}, a_1, b_1, c_1$ and RMSE) for different land cover classes based on reference sites for each land cover category.

i	the ith Landsat Band
$a_{0,i}$	coefficient for overall value for the ith Landsat Band (Eq. 3)
$c_{0,i}$	coefficient inter-annual change for the ith Landsat Band (Eq. 3)
$\overline{\rho}(i)$	overall spectral value at the center of each time series model for the ith Landsat Band.

4. Results

4.1. Results of the CCDC algorithm

The CCDC algorithm is capable of providing land cover change and classification maps continuously as newly collected Landsat
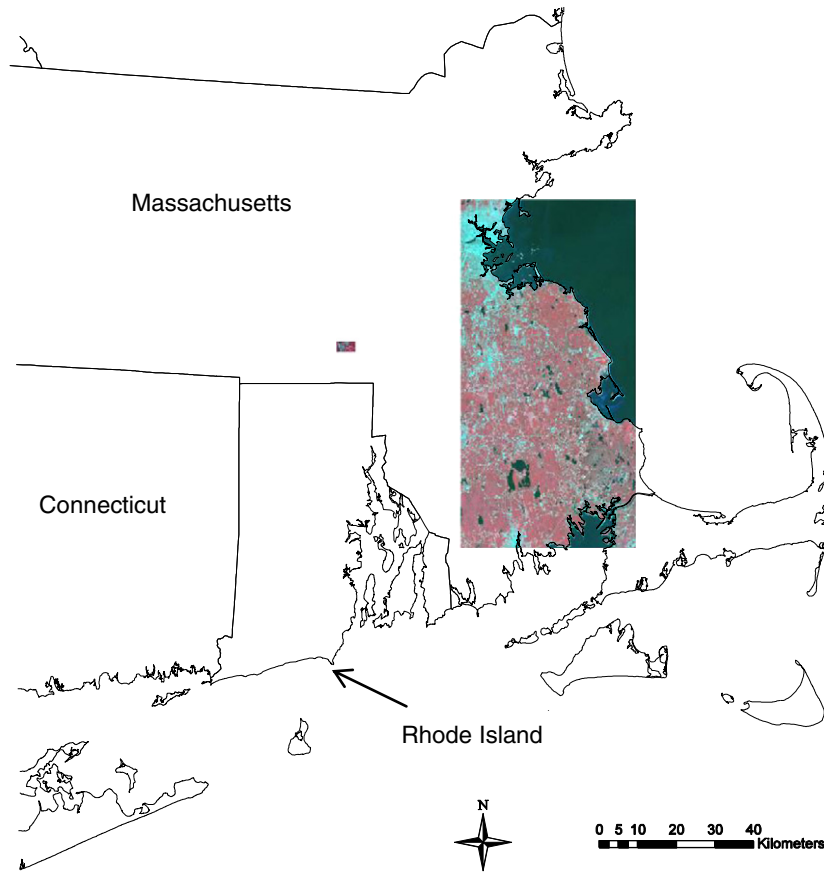
Fig. 10. Two pieces of Landsat data used for illustration the CCDC results in the study area. The smaller one (left) is used for illustrating the CCDC results in Fig. 11 and the larger one (right) is used for illustrating the CCDC results in Fig. 12.

images become available. We used a very small (5.6 km × 2.8 km) and a relatively large (90 km × 45 km) area to illustrate the results of the CCDC algorithm (Fig. 10).

Fig. 11 illustrates two "snapshots" of the CCDC results for the smaller piece of Landsat image. Fig. 11A is the CCDC result for September 2nd, 1988 and Fig. 11B is the CCDC result for July 16th, 2011. For each time period, the top three panels consist of a small piece of a newly collected Landsat image (left), the most recent land cover change map at the corresponding time (middle), and a land cover classification map at the same time (right). The three graphs at the bottom are the time series data (Band 4) for the three pixels located in sites 1, 2, and 3 that ultimately underwent some kinds of land cover change. That change that occurred at these pixels is obvious when viewed from the perspective of the entire time series. This approach allows the identification of the timing of each change, as well as the kind of change. When the time series has been built for a pixel and analyzed for change, it is possible to use the estimated time series models between the changes to identify the land cover class for the pixel at different time periods. For the pixel located at site 1, the estimated model preceding the change in 1988 can be used to classify the land cover for the entire time prior to the change. Similarly the estimated model subsequent to the change can be used to identify what land cover came after the change in 1988. The shape of the time series model can be very helpful in land cover classification which is evident in the time series graphs at the bottom, as initially both pixels located at sites 1 and 3 were conifer forest and pixel located at site 2 was a hardwood forest, and they are readily distinguishable by the difference in the amplitude of their time series in Band 4.

Fig. 12 illustrates the CCDC results for the larger piece of Landsat data. The two images on the left (Fig. 12A & B) are two clear Landsat images at the beginning (September 17th, 1984) and at the end (July 16th,

2011) of the time series. The two images on the right (Fig. 12C & D) are the most recent change detection and classification maps at the end of the time series generated by the CCDC algorithm. This comprehensive analysis of land cover provides both the timing and nature of land cover changes. To simplify for illustration purposes we collapsed the 16-categories land cover classes into 7-categories classes: *forest*, *wetland*, *agriculture*, *barren*, *water*, *grass*, and *developed*. For example, we can easily derive information like in the past 30 years the largest loss of *forest* is from *forest* to *developed* and the largest gain of *forest* is from *barren* to *forest* for this area. It can also provide new kinds of information about what kind of land cover change occurred on a yearly basis for the entire scene. Fig. 13 illustrates the annual amounts (km²) of different kinds of forest-related land cover change. Fig. 14 illustrates the amount of forest loss on a yearly basis. Note that both Figs. 13 and 14 start in 1986 instead of 1982 when first Landsat image is acquired. This is because the CCDC algorithm needs at least 15 clear observations to initialize the time series model for continuous change detection and classification and before 1986 most of the pixels do not have more than 15 clear observations.

4.2. Accuracy assessment

4.2.1. Accuracy assessment for change detection

As the CCDC algorithm is capable of detecting change at high temporal frequency, it is difficult to find reference data that can thoroughly assess its accuracy both spatially and temporally. There simply are not independent datasets available that have both finer spatial resolution and higher temporal frequency than Landsat images over the time period covered by Landsat. To know where and when land cover change occurs, the primary source for reference data is the Landsat images themselves (Cohen, Yang, & Kennedy, 2010). High spatial resolution
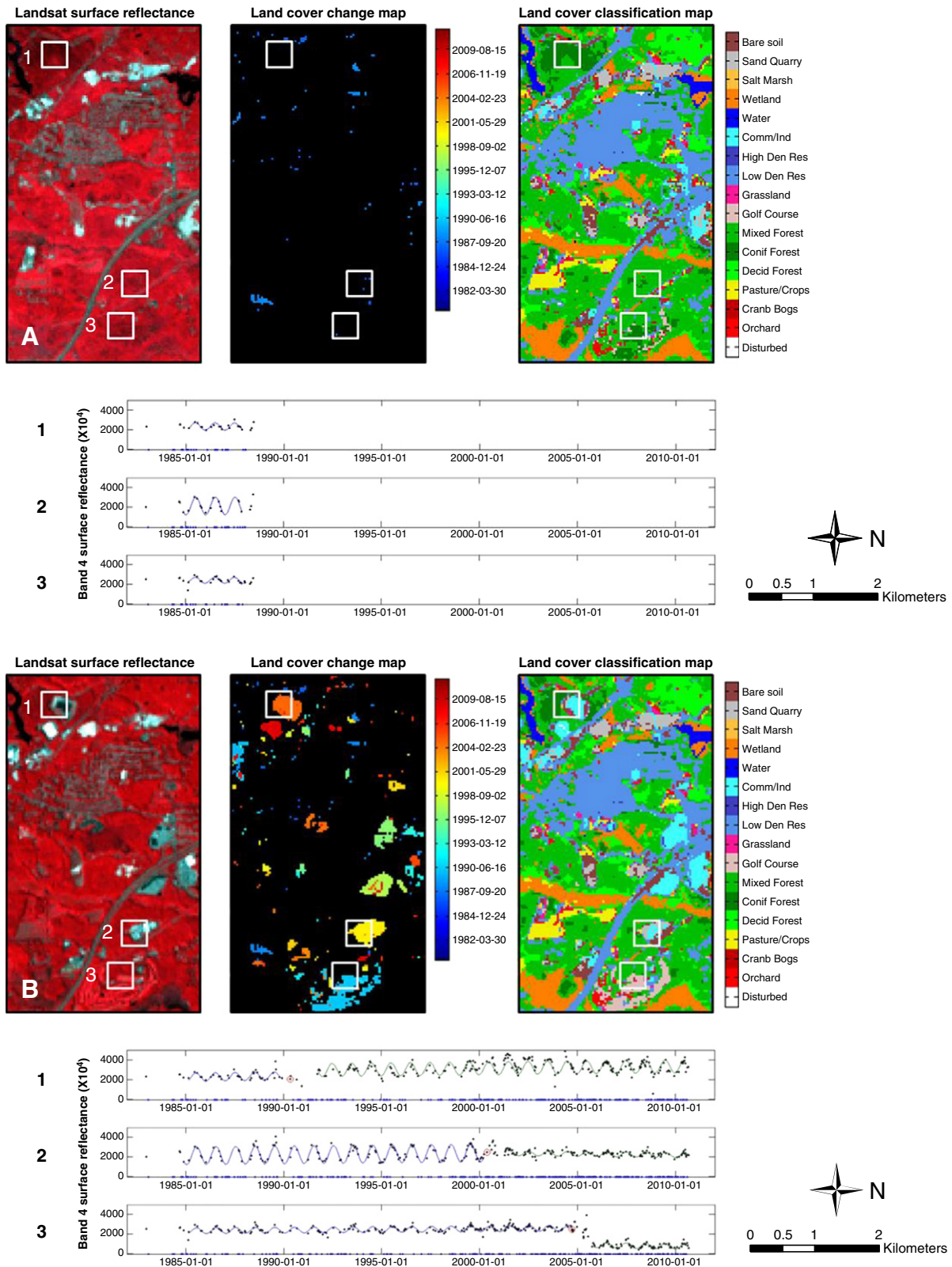
Fig. 11. Two "snapshots" of the smaller piece of Landsat data used for illustrating the CCDC results. Panel A is the CCDC results at the beginning (September 2nd, 1988) and panel B is the CCDC results at the end (July 16th, 2011) of the almost 30 years of time series data. For each time period, the top three panels are a small piece of a newly collected Landsat image (left), a map showing the timing and location of land cover change at the same time (middle), and the corresponding land cover map (right). The three graphs at the bottom are the time series of Band 4 surface reflectance for the three pixels in sites 1, 2, and 3 located in the center of the white rectangles. Note that all three sites underwent land cover change (they started as forest) and it is relatively easy to tell when they changed.

images from Google Earth (http://earth.google.com/) can help manual interpretation of the land cover classes. Though the high spatial resolution images cannot provide the same temporal frequency as Landsat data, their high spatial resolution is helpful in determining land cover change at longer time intervals. A random stratified sample design was used for assessing the change detection accuracy. A total of 500
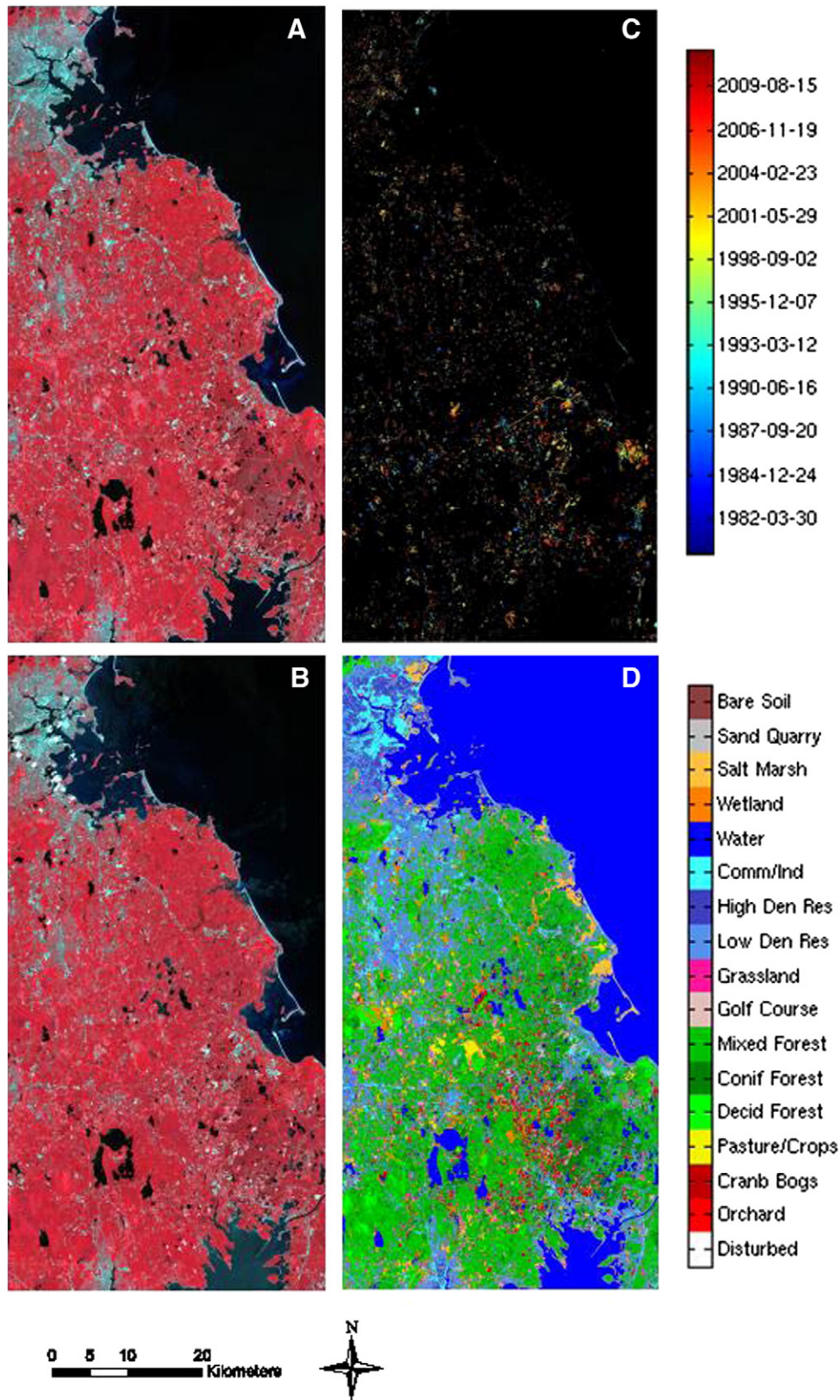
Fig. 12. The larger piece of Landsat data used for illustrating the CCDC results. Panel A is from the September 17th, 1984 Landsat image. Panel B is from the July 16th, 2011 Landsat image. Panel C is the most recent land cover change map. Panel D is the most recent land cover classification map.

reference pixels were selected, in which 250 pixels were from areas where land cover was persistent throughout the time of the analysis (1982–2011) and 250 pixels were selected within areas where land cover change was identified by the CCDC algorithm. By carefully

examining the time series data for all seven bands, it can be quite easy to identify pixels that have changed and when the change occurred. If there is confusion in determining a change or when it occurred, we examined the Landsat images before and after the possible change
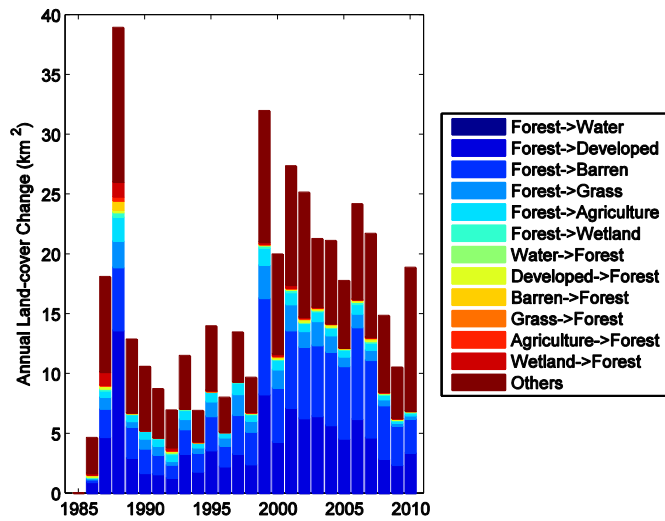
Fig. 13. Histogram of the annual amounts (km^2) of different kinds of forest-related land cover change between 1986 and 2010.

time or used high spatial resolution images from Google Earth to help determine what was happening at that time for that specific location. If there are multiple changes within one pixel, only the first change is used in the accuracy assessment.

The results of the accuracy assessment show producer's accuracy of 97.72% and user's accuracy of 85.60% for changed pixels, and overall accuracy of 91.80% (Table 3). The relative lower user's accuracy indicates more commission errors than omission errors in detected changes. A higher threshold or more consecutive observations may better balance the commission and omission errors.

The omission errors are mostly due to the following reasons: 1) partially changed pixels; and 2) change occurs too early, before the model is initialized. The partially changed pixels are always difficult to detect, as the magnitude of change is mostly dependent on the proportion of change within that pixel. In Fig. 15, there was a partial forest cut around 1998 and it is evident that after that point in time the Band 5 variability changed significantly, but the magnitude of this change is relatively small. On the other hand, if change occurred at the beginning of model initialization, the CCDC algorithm was unable to detect any kind of change as there are not enough observations to initialize the time series model (Fig. 16).

The commission errors mostly result from the following reasons: 1) overfitting of the time series model; 2) clouds missed three or
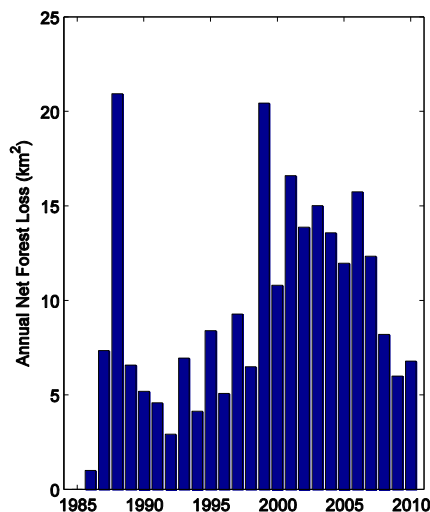

Fig. 14. Histogram of the annual amounts (km^2) of net forest loss between 1986 and 2010.

Table 3
The accuracy assessment of change detection in the spatial domain.

Reference data (spatial domain)				
	Changed pixels	Stable pixels	Total	User's (%)
Changed pixels	214	36	250	85.60
Stable pixels	5	245	250	98.00
Total	219	281		
Producer's (%)	97.72	87.19	Overall (%)	91.80

more times consecutively; 3) low temporal frequency of the time series data; and 4) very small RMSEs. Overfitting may cause serious problems. Though we are using simple time series model, overfitting can still happen if the data are always missing for a certain time of year because of clouds and/or snow. In Fig. 17, overfitting occurred for Band 4 at the beginning of model estimation, due to constant snow cover during the winter and this led to a commission error marked by the red circle. On the other hand, if clouds are missed three consecutive times, it will also be falsely identified as change (Fig. 18). For pixels located at the edges of Landsat images, the temporal frequency of the time series is much lower, and this will reduce the accuracy of model estimation, which may also lead to falsely identified change (Fig. 19). The last reason for false detection of change is a very small RMSE. Since the CCDC algorithm uses the RMSE value for defining the threshold for land cover change, when the RMSE value is small, a very slight change caused by the atmosphere or other factors can be easily confused with land cover change. This problem is common for pixels that are spectrally dark, such as *water* (Fig. 20). Some of these problems can be overcome by intelligent post-processing of the data. For example, if the land cover class is the same before and after the change is identified, it is likely that the identified change is an error.

The temporal accuracy of change detection was assessed for all 214 pixels in the accuracy assessment selected from areas where the algorithm found land cover change, and are correctly identified in the spatial domain. The proportion of the pixels that have the same change time between the CCDC results and the reference data is referred to as the "temporal accuracy". The algorithm occasionally finds change later than the reference data but it never found change earlier than the reference data. The proportion of the pixels that have the same time of change between the algorithm results and reference data is 79.91% (Table 4). The proportion of the pixels that are found to have changed later than the reference data but are within 32 days of the first date when a change is observable is 13.08% which is 65.12% of the temporal errors (Table 4). In other words, if we consider finding changes within a month of the first observable date is "correct", the temporal accuracy is as high as 92.99%.

The temporal errors are mostly due to the fact that at the very beginning of the change, the pixel may have only partially changed, and this spectral change is not large enough (less than three times the RMSE) to be identified by the CCDC algorithm. However, this change may be later identified by the CCDC algorithm when it is totally changed. In Fig. 21, before the red circle (the change identified by the CCDC algorithm), there is one observation that slightly deviates from model prediction that was mainly caused by a partial forest cut (indicated by the green circle), but this deviation is still relatively small compared to the next clear observation in the red circle.

Table 4
The accuracy assessment of change detection in the temporal domain.

Reference data (temporal domain)				
	Same	Late ≤ 32 days	Late > 32 days	Total
Changed pixels	171	28	15	214
Proportion (%)	79.91	13.08	7.01	100.00

Table 5
The accuracy assessment of classification.

	O	CB	PC	DF	CF	MF	GC	G	LD	HD	CI	W	WT	SM	SQ	BS	Use.
O	1986	0	128	1	0	0	43	71	22	0	0	0	0	0	0	33	86.95
CB	0	2152	2	0	0	3	8	0	0	0	0	5	0	0	0	2	99.08
PC	135	2	3550	3	0	0	39	93	14	0	0	0	12	0	17	106	89.40
DF	3	0	10	3619	11	209	34	5	26	0	9	0	21	0	0	14	91.37
CF	0	0	0	0	3643	431	10	0	8	0	0	1	0	0	0	0	89.01
MF	1	8	23	136	379	4686	23	12	39	0	73	20	42	14	15	39	85.05
GC	12	11	37	0	0	42	2450	83	3	0	0	0	0	0	0	24	92.42
G	51	0	60	0	0	21	109	2967	91	0	20	0	0	8	17	46	87.99
LD	32	13	110	0	34	0	24	117	2880	101	266	0	16	0	2	50	78.39
HD	0	0	0	0	0	0	0	13	185	1494	19	0	0	0	0	0	87.32
CI	0	0	0	0	0	0	0	61	44	136	3108	0	0	7	114	59	88.07
W	0	0	0	0	0	0	8	0	51	0	0	8311	65	3	0	0	98.49
WT	0	1	36	30	2	12	1	0	11	0	8	112	3431	42	5	9	92.73
SM	2	0	0	0	0	0	3	0	6	0	0	0	21	2987	0	0	98.94
SQ	0	0	0	46	0	32	0	34	5	16	165	13	0	0	2635	159	84.86
BS	6	22	72	24	3	0	0	66	39	0	51	12	1	0	87	2327	85.87
Pro.	89.14	97.42	88.13	93.78	89.46	86.20	89.03	84.24	84.11	85.52	83.57	98.08	95.07	97.58	91.11	81.14	90.20

Note: O = Orchards, CB = Cranberry Bogs, PC = Pasture/Row Crops, DF = Deciduous Forest, CF = Conifer Forest, MF = Mixed Forest, GC = Golf Course, G = Grassland, LD = Low Density Residential, HD = High Density Residential, CI = Commercial/Industrial, W = Water, WT = Wetland, SM = Salt Marsh, SQ = Sand Quarry, BS = Bare Soil.

4.2.2. Accuracy assessment for classification

The land cover reference data previously used for continuous land cover classification (introduced in Section 2.3) were used as the basis for assessing the accuracy of classification for the CCDC algorithm. As the land cover reference data were collected between 2005 and 2007, we will only assess the accuracy of land cover classification at this specific time interval. A total of 80% of the land cover reference data were randomly selected to train the classifier, and the remaining 20% were used to assess map accuracy (Fielding & Bell, 1997). This process was repeated 50 times and the average user's accuracy, average producer's accuracy, and average overall classification accuracy were used to assess the land cover classification accuracy for the CCDC algorithm. In this approach, each reference pixel is used many times for both training and accuracy assessment, but never both for a single trial. The average of the overall accuracy of the land cover classification with 16-categories is 90.20% (Table 5), which is almost the same accuracy as another study of the same place using all available dimensions (spectral, temporal, and spatial) of Landsat data (Zhu, Woodcock, Rogan, et al., 2012). The average producer's and user's accuracies for the different land cover types are also quite high, with mostly being approximately 90% (Table 5). The largest confusions are between *Mixed Forest* and *Conifer Forest*, *Deciduous Forest* and *Mixed Forest*, *Low Density Residential* and *High Density Residential*, and *Low Density Residential* and *Commercial/Industrial* (Table 5).

5. Discussion and conclusions

Detection of land cover change and classification are difficult problems in remote sensing. Better use of the temporal domain of Landsat data can improve both change detection and land cover classification. In this study, we developed a new algorithm for continuous change detection and classification at high temporal frequency. By using all available Landsat data, this approach allows reconstruction of the history of the Earth surface in the Landsat TM and ETM + era. Models estimated by sines and cosines can predict Landsat observations at any date assuming there is no land cover change. The CCDC algorithm flags land cover change by differencing the predicted and observed Landsat data. It determines a pixel has experienced a land cover change if it shows "change" for three consecutive times. The estimated time series coefficients (also including the RMSEs) were used for land cover classification. The reference data revealed that the CCDC results were accurate for detecting land cover change, with producer's accuracy of 97.72% and user's accuracies of 85.60% in the spatial domain, and temporal accuracy of 79.91%. The CCDC classification results also showed high overall accuracy of 90.20%.

The CCDC algorithm has many advantages. It is fully automated and is capable of monitoring many kinds of land cover change as soon as new images become available. Moreover, there are no empirical or global thresholds used in detecting change. The thresholds are generated through the original observations and model estimation which are done separately for each individual pixel. In this study, three times the RMSE is recommended for thresholding, but more subtle changes can be captured if two times the RMSE is used, which also result in more false detection of land cover change. The continuous character of the monitoring makes the algorithm capable of using as many images as possible. Therefore, how fast the CCDC algorithm is able to find change and its corresponding land cover type is primarily dependent on the frequency of available clear observations. This algorithm will improve as the frequency of images from sensors like Landsat increases (Arvidson et al., 2006). The opening of the archive from Earth Resources Observation and Science (EROS) Data Center is the first major step. Data from the Landsat 8 should further increase the frequency of available observations considering the much larger duty cycle for Landsat 8 compared with previous Landsat satellites. The two Sentinel 2A/2B satellites are very similar to Landsat (Drusch et al., 2012). They have a Sun-synchronous orbit at 786 km and a 10:30 a.m. descending node,
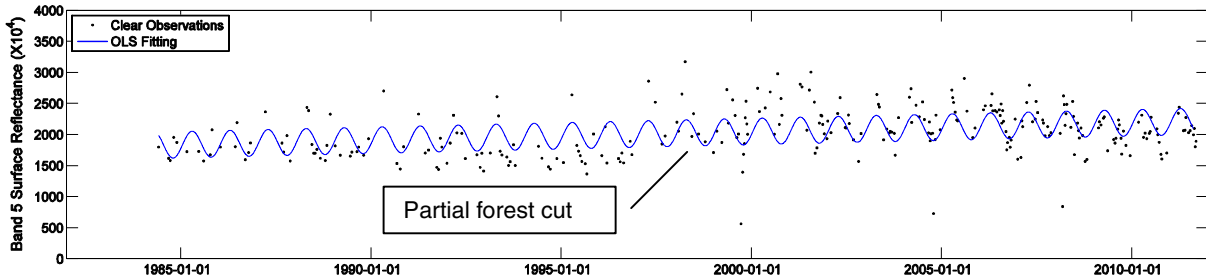
Fig. 15. Omission error in change detection for CCDC: partial forest cut illustrated by time series Band 5 surface reflectance.
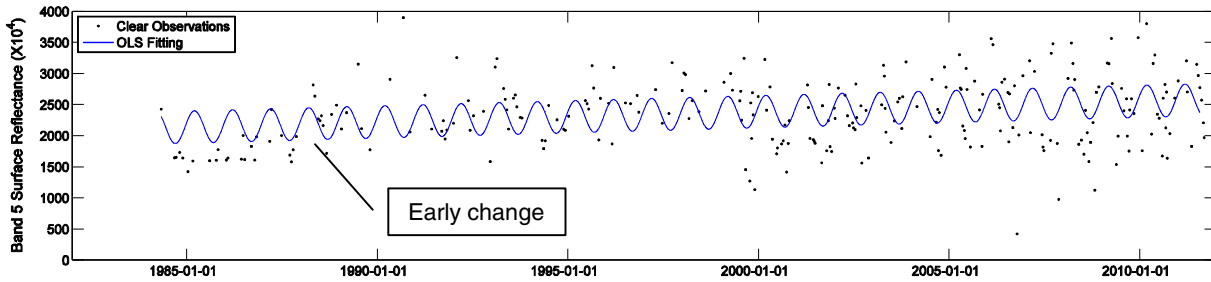

Fig. 16. Omission error in change detection for CCDC: change occurred too early illustrated by time series Band 5 surface reflectance.

which is close to the Landsat local overpass time. The 13 spectral bands span from the visible and the NIR to the SWIR and include all six Landsat bands and at similar spatial resolution. Though there are some differences in widths and locations of the spectral bands and spatial resolutions between Landsat and Sentinel 2A/2B (Drusch et al., 2012), with some modifications or adjustments of the algorithm, it will be possible to combine observations from Sentinel 2A/2B with Landsat observations in the CCDC algorithm. With Sentinel 2A planned for launch in 2014 and the second (2B) planed for launch 18 month later, there will be 5 days repeat time for observations at the Equator and 2–3 days at mid-latitudes (Berger, Moreno, Johannessen, Levelt, & Hanssen, 2012). More importantly, the Sentinel data policy is free and open access to
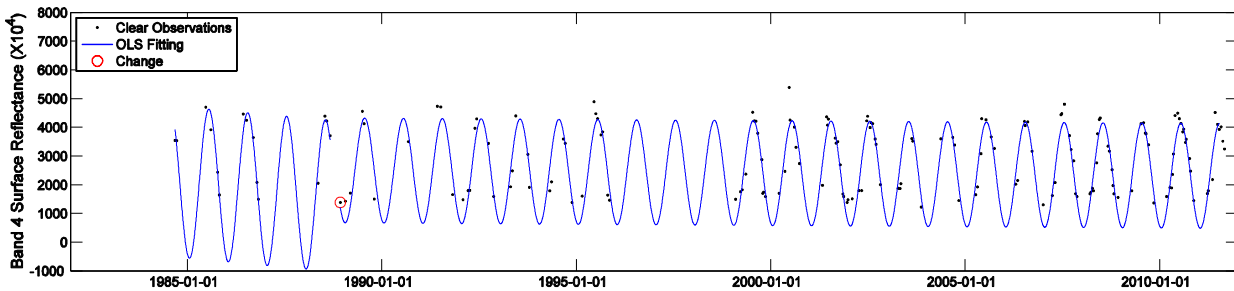

Fig. 17. Commission error in change detection for CCDC: overfitting of time series model illustrated by time series Band 4 surface reflectance. The red circle indicates the incorrect assignment of change.
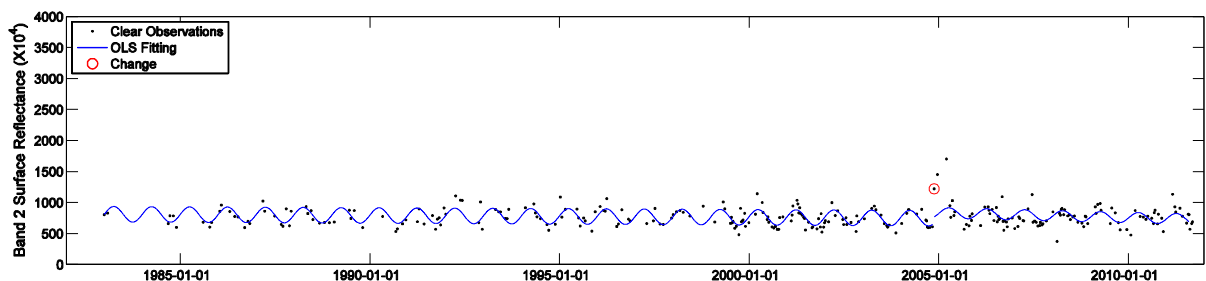

Fig. 18. Commission error in change detection for CCDC: clouds missed three times consecutively illustrated by time series Band 2 surface reflectance. The red circle indicates the incorrect assignment of change.
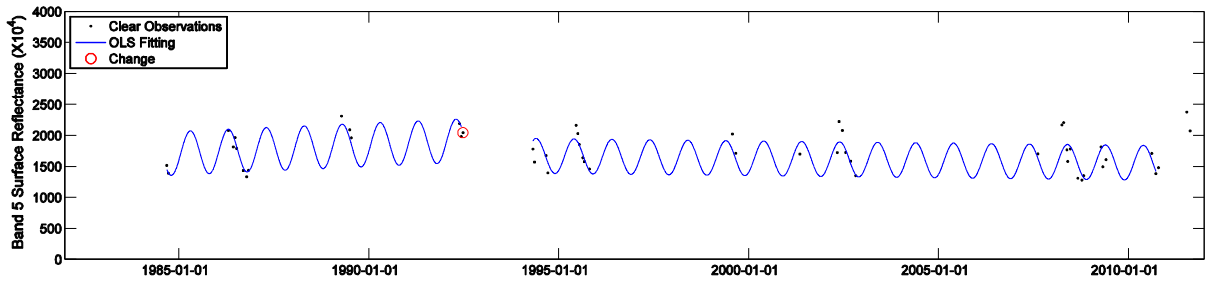
Fig. 19. Commission error in change detection for CCDC: low temporal frequency of the time series data illustrated by time series Band 5 surface reflectance. The red circle indicates the incorrect assignment of change.
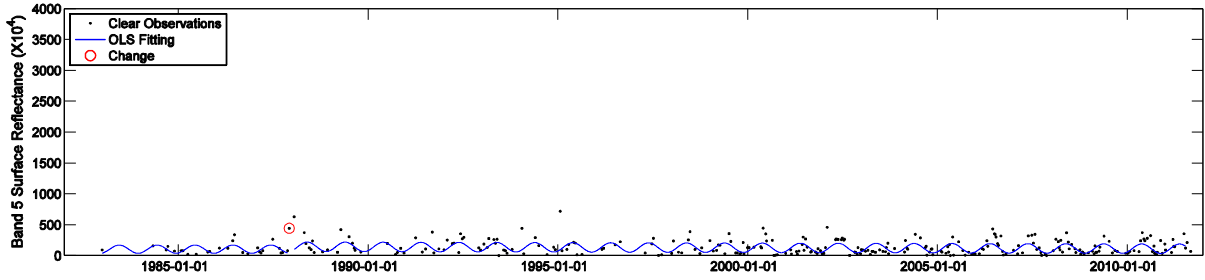

Fig. 20. Commission error in change detection for CCDC: small RMSE illustrated by time series Band 5 surface reflectance. The red circle indicates the incorrect assignment of change.

users. In principle, anybody can access acquired Sentinel data and there is no difference between public, commercial and scientific use and between European and non-European users (Aschbacher & Milagro-Pérez, 2012). By combining combined with Landsat 7 and 8, and two Sentinel 2A and 2B, there would be typically 10 high resolution observations per month, greatly improving the availability of Landsat-like

observations such that we will be able to begin to monitor change in near real-time at Landsat scales.

By using all available observations and considering each pixel separately, the CCDC algorithm can overcome limitations like the failure of the Scan Line Corrector (SLC) in Landsat 7 as the scan line gaps are treated like clouds, cloud shadows, or snow and only the available
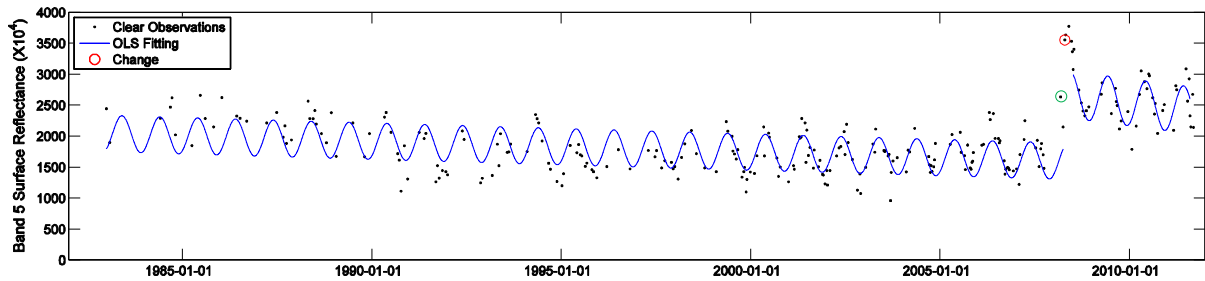

Fig. 21. Temporal error in change detection for CCDC: finding change later than it is observed in the reference data. The red circle is the "first" changed observation identified by the CCDC algorithm and the green circle is the first time the change (a partial forest cut) can be observed in close examination of the images.
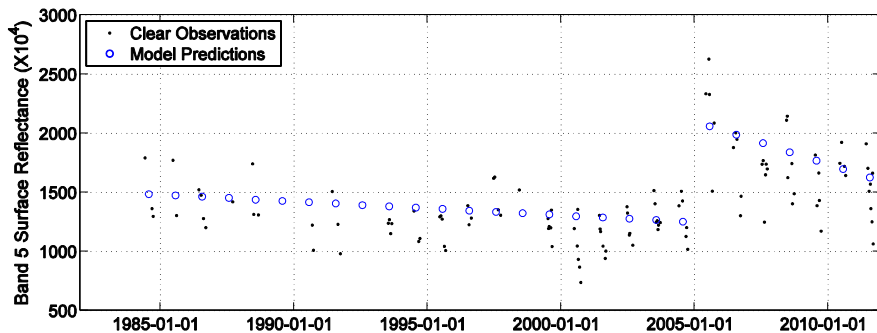

Fig. 22. Clear observations (Band 5) from Jun. to Sept. and model predictions for Aug. 1st every year between 1984 and 2011. Forest clearing occurred in 2005 for this pixel.

clear observations are used. This approach allows use of images from all times of year or that are partially cloudy. It also can work in very heterogeneous areas that are reported to be problematic for some methods (Huang et al., 2010; Masek et al., 2008). Moreover, the CCDC algorithm does not need to perform relative normalization for each image like many methods (Huang et al., 2010; Kennedy et al., 2007), as the time series model already includes the effects of phenology and sun angle differences. By using many observations for model estimation, this algorithm is not adversely affected by noise and the predicted data form a more stable basis for comparison with new observations. Fig. 22 illustrates the model-predicted Landsat observations at the same time of year and the original clear Landsat observations during growing season (from June to September) through the TM and ETM + era for a deforestation pixel. It is clear that the model predicted observations are much more stable compared to the original observations and this feature should significantly reduce false positive errors in change detection.

Additionally, land cover maps from any time period in the history of the Landsat 4–8 era can be generated. More specifically, this algorithm can also generate maps of land cover change over any specified time period and provide information about the land cover categories before and after change occurs by simply differencing the two land cover maps generated by CCDC at different time. Usually, it is very dangerous to compare two land cover maps from two different time to find change, as the areas of land cover change are relatively small compared to the magnitude of errors in land cover classification maps. This algorithm avoids this problem when comparing two land cover maps to find change, as the land cover classification algorithm is based on the results of change detection. Moreover, this algorithm can also provide information about inter-annual changes via the trend coefficients. It is possible to provide new land cover categories that are unique temporally, for example, the *forest* class can be separated into *growing forest*, *mature forest*, and *declining forest*. This kind of information is important for the study of vegetation health conditions and for carbon modeling, but difficult to derive from the conventional land cover classification methods.

The CCDC algorithm also has limitations. First of all, this algorithm is computationally expensive and needs lots of data storage. Just the surface reflectance and brightness temperature data takes more than 500 gigabytes for a total of 519 Landsat images. The algorithm updates the time series model every time new observations are available, which has the benefit of more accurate model estimation, but also greatly increases the computational load. Second, this algorithm requires high temporal frequency of clear observations. For places of persistent snow or clouds, the model estimation may not be accurate as there are not enough observations to estimate the time series model. For extreme cases, if there are less than 15 clear observations, the CCDC algorithm will not be able to initialize the time series model. For places outside of the United States this problem will be more common. Third, we assume that the simple sinusoidal model is able to estimate all kinds of land cover types, which may not be valid for land cover types that have more intra-annual variation, such as agriculture. A more complex time series model is needed if we want to apply it to other parts of the world. Finally, though the data-driven threshold used in this algorithm is able to handle many kinds of land cover change for the Boston scene, it may have problems for places that have large inter-annual variations. For example semi-arid regions that exhibit high variability in the timing of phenological processes may prove particularly challenging, as the data will fluctuate more at some times of the year and at this time a higher threshold is needed. Thresholds able to change temporally may provide better accuracy.

Acknowledgments

References

Anderson, J. R. (1976). *A land use and land cover classification system for use with remote sensor data, Vol. 964.* US Government Printing Office.

Arvidson, T., Goward, S., Gasch, J., & Williams, D. (2006). Landsat-7 long-term acquisition plan: Development and validation. *Photogrammetric Engineering & Remote Sensing, 72*(10), 1137–1146.

Aschbacher, J., & Milagro-Pérez, M. P. (2012). The European Earth monitoring (GMES) programme: Status and perspectives. *Remote Sensing of Environment, 120*, 3–8.

Berger, M., Moreno, J., Johannessen, J. A., Levelt, P. F., & Hanssen, R. F. (2012). ESA's sentinel missions in support of Earth system science. *Remote Sensing of Environment, 120*, 84–90.

Breiman, L. (2001). Random forests. *Machine Learning, 45*, 5–32.

Brooks, E. B., Thomas, V. A., Wynne, R. H., & Coulston, J. W. (2012). Fitting the multitemporal curve: A fourier series approach to the missing data problem in remote sensing analysis. *Geoscience and Remote Sensing, 50*(9), 3340–3353.

Carrao, H., Goncalves, P., & Caetano, M. (2008). Contribution of multispectral and multitemporal information from MODIS images to land cover classification. *Remote Sensing of Environment, 112*(3), 986–997.

Cohen, W. B., Yang, Z., & Kennedy, R. (2010). Detecting trends in forest disturbance and recovery using yearly Landsat time series: 2. TimeSync—Tools for calibration and validation. *Remote Sensing of Environment, 114*(12), 2911–2924.

Collins, J. B., & Woodcock, C. E. (1996). An assessment of several linear change detection techniques for mapping forest mortality using multitemporal Landsat TM data. *Remote Sensing of Environment, 56*, 66–77.

Coppin, P. R., & Bauer, M. E. (1996). Digital change detection in forest ecosystems with remote sensing imagery. *Remote Sensing Reviews, 13*(3–4), 207–234.

Coppin, P., Jonckheere, I., Nackaerts, K., Muys, B., & Lambin, E. (2004). Digital change detection methods in ecosystem monitoring: A review. *International Journal of Remote Sensing, 25*(9), 1565–1596.

Drusch, M., Del Bello, U., Carlier, S., Colin, O., Fernandez, V., Gascon, F., et al. (2012). Sentinel-2: ESA's optical high-resolution mission for GMES operational services. *Remote Sensing of Environment, 120*, 25–36.

DuMouchel, W. H., & O'Brien, F. L. (1989). Integrating a robust option into a multiple regression computing environment. *Computer Science and Statistics: Proceedings of the 21st Symposium on the Interface*. Alexandria, VA American Statistical Association.

Eklundh, L., Johansson, T., & Solberg, S. (2009). Mapping insect defoliation in Scots pine with MODIS time-series data. *Remote Sensing of Environment, 113*(7), 1566–1573.

Fielding, A. H., & Bell, A. J. F. (1997). A review of methods for the assessment of prediction errors in conservation presence/absence models. *Environmental Conservation, 24*(1), 38–49.

Foody, G. M. (2002). Status of land cover classification accuracy assessment. *Remote Sensing of Environment, 80*(1), 185–201.

Friedl, M.A., McIver, D. K., Hodges, J. C. F., Zhang, X. Y., Muchoney, D., Strahler, A. H., et al. (2002). Global land cover mapping from MODIS: Algorithms and early results. *Remote Sensing of Environment, 83*(1), 287–302.

Friedl, M.A., Menashe, D. S., Tan, B., Schneider, A., Ramankutty, N., Sibley, A., et al. (2010). MODIS collection 5 global land cover: Algorithm refinements and characterization of new datasets. *Remote Sensing of Environment, 114*, 168–182.

Fuller, R. M., Smith, G. M., & Devereux, B. J. (2003). The characterisation and measurement of land cover change through remote sensing: Problems in operational applications? *International Journal of Applied Earth Observation and Geoinformation, 4*(3), 243–253.

Galford, G. L., Mustard, J. F., Melillo, J., Gendrin, A., Cerri, C. C., & Cerri, C. E. P. (2008). Wavelet analysis of MODIS time series to detect expansion and intensification of row-crop agriculture in Brazil. *Remote Sensing of Environment, 112*(2), 576–587.

Goodwin, N. R., Coops, N. C., Wulder, M.A., Gillanders, Schroeder, T. A., & Nelson, T. (2008). Estimation of insect infestation dynamics using a temporal sequence of Landsat data. *Remote Sensing of Environment, 112*, 3680–3689.

Gopal, S., Woodcock, C. E., & Strahler, A. (1999). Fuzzy neural classification of global land cover from a 1 degree AVHRR Data Set. *Remote Sensing of Environment, 67*, 230–243.

Guerschman, J. P., Paruelo, J. M., Bella, C. D. I., Giallorenzi, M. C., & Pacin, F. (2003). Land cover classification in the Argentine Pampas using multi-temporal Landsat TM data. *International Journal of Remote Sensing, 24*(17), 3381–3402.

Hansen, M. C., Defries, R. S., Townshend, J. R. G., & Sohlberg, R. (2000). Global land cover classification at 1 km spatial resolution using a classification tree approach. *International Journal of Remote Sensing, 21*(6 & 7), 1331–1364.

Hansen, M. C., Potapov, P. V., Moore, R., Hancher, M., Turubanova, S. A., Tyukavina, A., et al. (2013). High-resolution global maps of 21st-century forest cover change. *Science, 342*(6160), 850–853.

Healey, S., Cohen, W. B., Yang, Z., & Krankina, O. N. (2005). Comparison of Tasseled Cap-based Landsat data structure for use in forest disturbance detection. *Remote Sensing of Environment, 97*, 301–310.

Holland, P. W., & Welsch, R. E. (1977). Robust regression using iteratively reweighted least-squares. *Theory and Methods*, 813–827.

Homer, C., Huang, C., Yang, L., Wylie, B., & Coan, M. (2004). Development of a 2001 national land-cover database for the United States. *Photogrammetric Engineering & Remote Sensing, 70*(7), 829–840.

Hostert, P., Röder, Achim, & Hill, J. (2003). Coupling spectral unmixing and trend analysis for monitoring of long-term vegetation dynamics in Mediterranean rangelands. *Remote Sensing of Environment, 87*, 183–197.

Huang, C., Goward, S. N., Masek, J. G., Thomas, N., Zhu, Z., & Vogelmann, J. E. (2010). An automated approach for reconstructing recent forest disturbance history using dense Landsat time series stacks. *Remote Sensing of Environment, 114*, 183–198.

Jensen, J. R., Rutchey, K., Koch, M. S., & Narumalani (1995). Inland wetland change detection in the everglades water conservation area 2A using a time series of

normalized remotely sensed data. *Photogrammetric Engineering & Remote Sensing, 61*(2), 199–209.

Jin, S., & Sader, S. A. (2005). MODIS time-series imagery for forest disturbance detection and quantification of patch size effects. *Remote Sensing of Environment, 99*(4), 462–470.

Jung, M., Henkel, K., Herold, M., & Churkina, G. (2006). Exploiting synergies of global land cover products for carbon cycle modeling. *Remote Sensing of Environment, 101*(4), 534–553.

Kennedy, R. E., Cohen, W. B., & Schroeder, T. A. (2007). Trajectory-based change detection for automated characterization of forest disturbance dynamics. *Remote Sensing of Environment, 110*, 370–386.

Kennedy, R. E., Yang, Z., & Cohen, W. B. (2010). Detecting trends in forest disturbance and recovery using yearly Landsat time series: 1. LandTrendr—Temporal segmentation algorithms. *Remote Sensing of Environment, 114*(12), 2897–2910.

Lambin, E. F., & Strahler, A. H. (1994). Change-vector analysis in multitemporal space: A tool to detect and categorize land-cover change processes using high temporal-resolution satellite data. *Remote Sensing of Environment, 48*, 231–244.

Lark, R. M., & Stafford, J. V. (1997). Classification as a first step in the interpretation of temporal and spatial variation of crop yield. *Annals of Applied Biology, 130*(1), 111–121.

Loveland, T. R., Reed, B. C., Brown, J. F., Ohlen, D. O., Zhu, Z., Yang, L. W. M. J., & Merchant, J. W. (2000). Development of a global land cover characteristics database and IGBP DISCover from 1 km AVHRR data. *International Journal of Remote Sensing, 21*(6–7), 1303–1330.

Lunetta, R. S., Knight, J. F., Ediriwickrema, J., Lyon, J. G., & Worthy, L. D. (2006). Land-cover change detection using multi-temporal MODIS NDVI data. *Remote Sensing of Environment, 105*(2), 142–154.

Masek, J. G., Huang, C., Wolfe, R., Cohen, W., Hall, F., Kutler, J., et al. (2008). North American forest disturbance mapped from decadal Landsat record. *Remote Sensing of Environment, 112*, 2914–2926.

Masek, J. G., Vermote, E. F., Saleous, N., Wolfe, R., Hall, E. F., Huemmrich, F., et al. (2006). A Landsat surface reflectance data set for North America, 1990–2000. *Geoscience and Remote Sensing Letters, 3*, 68–72.

Melaas, E. K., Friedl, M.A., & Zhu, Z. (2013). Detecting interannual variation in deciduous broadleaf forest phenology using Landsat TM/ETM + data. *Remote Sensing of Environment, 132*, 176–185.

O'Leary, D. P. (1990). Robust regression computation using iteratively reweighted least squares. *Society for Industrial and Applied Mathematics, 11*(3), 466–480.

Pflugmacher, D., Cohen, W. B., & E Kennedy, R. (2012). Using Landsat-derived disturbance history (1972–2010) to predict current forest structure. *Remote Sensing of Environment, 122*, 146–165.

Rogan, J., Bumbarger, N., Kulakowski, D., Christman, Z. J., Runfola, D.M., & Blanchard, S. D. (2010). Improving forest type discrimination with mixed lifeform classes using fuzzy classification thresholds informed by field observations. *Canadian Journal of Remote Sensing, 36*(6), 699–708.

Rogan, J., Franklin, J., & Roberts, D. A. (2002). A comparison of methods for monitoring multitemporal vegetation change using Thematic Mapper imagery. *Remote Sensing of Environment, 80*, 143–156.

Roy, D. P., Jin, Y., Lewis, P. E., & Justice, C. O. (2005). Prototyping a global algorithm for systematic fire-affected area mapping using MODIS time series data. *Remote Sensing of Environment, 97*(2), 137–162.

Schaaf, C. B., Gao, F., Strahler, A. H., Lucht, W., Li, X., Tsang, T., et al. (2002). First operational BRDF, albedo nadir reflectance products from MODIS. *Remote Sensing of Environment, 83*(1), 135–148.

Seto, K. C., Woodcock, C. E., Song, C., Huang, X., Lu, J., & Kaufmann, R. K. (2002). Monitoring land-use change in the Pearl River Delta using Landsat TM. *International Journal of Remote Sensing, 23*(10), 1985–2004.

Singh, A. (1989). Review Article Digital change detection techniques using remotely-sensed data. *International Journal of Remote Sensing, 10*(6), 989–1003.

Street, J. O., Carroll, R. J., & Ruppert, D. (1988). A note on computing robust regression estimates via iteratively reweighted least squares. *American Statistical Association, 42*(2), 152–154.

Tan, B., Woodcock, C. E., Hu, J., Zhang, P., Ozdogan, M., Huang, D., et al. (2006). The impact of gridding artifacts on the local spatial properties of MODIS data: Implications for validation, compositing, and band-to-band registration across resolution. *Remote Sensing of Environment, 105*(2), 98–114.

Tucker, C. J., Townshend, J. R. G., & Goff, T. E. (1985). African land-cover classification using satellite data. *Science, 227*(4685), 369–375.

Verbesselt, J., Hyndman, R., Newnham, G., & Culvenor, D. (2010). Detecting trend and seasonal changes in satellite image time series. *Remote Sensing of Environment, 114*(1), 106–115.

Vermote, E. F., El Saleous, N., Justice, C. O., Kaufman, Y. J., Privette, J. L., et al. (1997). Atmospheric correction of visible to middle-infrared EOS-MODIS data over land surfaces: Background, operational algorithm, and validation. *Journal of Geophysical Research, 102*, 17131–17141.

Vogelmann, J. E., Tolk, B., & Zhu, Z. (2009). Monitoring forest changes in the southwestern United States using multitemporal Landsat data. *Remote Sensing of Environment, 113*, 1739–1748.

Wolter, P. I., Mladenoft, D. S., & Crow, T. R. (1995). Improved forest classification in the northern lake states using multi-temporal Landsat imagery. *Photogrammetry Engineering & Remote Sensing, 61*(9), 1129–1143.

Woodcock, C. E., Allen, R., Anderson, M., Belward, A., Bindschadler, R., Cohen, W., et al. (2008). Free access to Landsat imagery. *Science, 320*(5879), 1011.

Woodcock, C. E., Macomber, S. A., Pax-Lenney, M., & Cohen, W. B. (2001). Large area monitoring of temperate forest change using Landsat data: Generalization across sensors, time and space. *Remote Sensing of Environment, 78*(1–2), 194–203.

Woodcock, C. E., & Strahler, A. H. (1987). The factor of scale in remote sensing. *Remote Sensing of Environment, 21*(3), 311–332.

Wulder, M.A., White, J. C., Goward, S. N., Masek, J. G., Irons, J. R., Herold, M., et al. (2008). Landsat continuity: Issues and opportunities for land cover monitoring. *Remote Sensing of Environment, 112*(3), 955–969.

Xin, Q., Olofsson, P., Zhu, Z., Tan, B., & Woodcock, C. E. (2012). Towards near real-time monitoring of forest disturbance by fusion of MODIS and Landsat data. *Remote Sensing of Environment, 135*, 234–247.

Zhang, Y., Rossow, W. B., Lacis, A. A., Oinas, V., & Mishchenko, M. I. (2004). Calculation of radiative fluxes from the surface to top of atmosphere based on ISCCP and other global data sets: Refinements of the radiative transfer model and the input data. *Journal of Geophysical Research, 109*(19), 19105.

Zhu, Z., & Woodcock, C. E. (2012). Object-based cloud and cloud shadow detection in Landsat imagery. *Remote Sensing of Environment, 118*(15), 83–94.

Zhu, Z., & Woodcock, C. E. (2014). *Automated cloud, cloud shadow, and snow detection based on multitemporal Landsat data: An algorithm designed specifically for monitoring surface change, submitted to Remote Sensing of Environment.*

Zhu, Z., Woodcock, C. E., & Olofsson, P. (2012). Continuous monitoring of forest disturbance using all available Landsat imagery. *Remote Sensing of Environment, 122*, 75–91.

Zhu, Z., Woodcock, C. E., Rogan, J., & Kellndorfer, J. (2012). Assessment of spectral, polarimetric, temporal, and spatial dimensions for urban and peri-urban land cover classification using Landsat and SAR data. *Remote Sensing of Environment, 117*, 72–82.